

REINFORCEMENT IN CERAMIC
MATRIX COMPOSITES

LIU, JENQ

DEGREE DATE: 1991

U·M·I Dissertation
Services

This is an authorized facsimile, made from the microfilm master copy of the original dissertation or masters thesis published by UMI.

The bibliographic information for this thesis is contained in UMI's Dissertation Abstracts database, the only central source for accessing almost every doctoral dissertation accepted in North America since 1861.

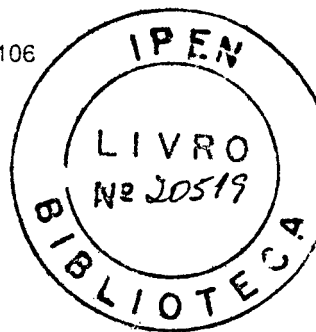
U·M·I Dissertation Services

A Bell & Howell Company

300 N. Zeeb Road, Ann Arbor, Michigan 48106

1-800-521-0600

313-761-4700



Printed in 1994 by xerographic process
on acid-free paper

COMISSÃO NACIONAL DE ENERGIA NUCLEAR/SP - IPEN

Order Number 9216448

Reinforcement in ceramic matrix composites

Liu, Jenq, Ph.D.

University of Missouri - Rolla, 1991

U·M·I
300 N. Zeeb Rd.
Ann Arbor, MI 48106

COMISSÃO NACIONAL DE ENERGIA NUCLEAR/SP - IPEN

INFORMATION TO USERS

This manuscript has been reproduced from the microfilm master. UMI films the text directly from the original or copy submitted. Thus, some thesis and dissertation copies are in typewriter face, while others may be from any type of computer printer.

The quality of this reproduction is dependent upon the quality of the copy submitted. Broken or indistinct print, colored or poor quality illustrations and photographs, print bleedthrough, substandard margins, and improper alignment can adversely affect reproduction.

In the unlikely event that the author did not send UMI a complete manuscript and there are missing pages, these will be noted. Also, if unauthorized copyright material had to be removed, a note will indicate the deletion.

Oversize materials (e.g., maps, drawings, charts) are reproduced by sectioning the original, beginning at the upper left-hand corner and continuing from left to right in equal sections with small overlaps. Each original is also photographed in one exposure and is included in reduced form at the back of the book.

Photographs included in the original manuscript have been reproduced xerographically in this copy. Higher quality 6" x 9" black and white photographic prints are available for any photographs or illustrations appearing in this copy for an additional charge. Contact UMI directly to order.

U·M·I

University Microfilms International
A Bell & Howell Information Company
300 North Zeeb Road, Ann Arbor, MI 48106-1346 USA
313/761-4700 800/521-0600

REINFORCEMENT IN CERAMIC MATRIX COMPOSITES

BY

JENQ LIU, 1958-

A DISSERTATION

Presented to the Faculty of the Graduate School of the

UNIVERSITY OF MISSOURI- ROLLA

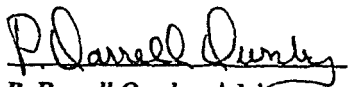
In Partial Fulfillment of the Requirement for the Degree

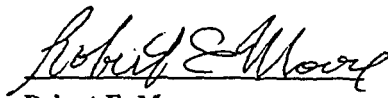
DOCTOR OF PHILOSOPHY IN CERAMIC ENGINEERING

1991

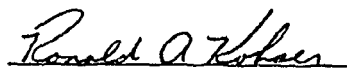
T6325
Copy 1
108 pages

Approved by


P. Darrell Ownby, Advisor


Robert E. Moore


Mohamed N. Rahaman


Ronald A. Kohser


Joseph W. Newkirk

PUBLICATION DISSERTATION OPTION

This dissertation has been prepared in the style utilized by the *Journal of the American Ceramic Society* and *Ceramic Engineering Science Proceedings*.

Paper 1 will be presented for publication in the *Journal of the American Ceramic Society*.

Paper 2 has recently been published in the *Journal of the American Ceramic Society*.

Paper 3 and 4 have recently been published in the *Ceramic Engineering Science Proceedings*.

Appendices A and B have already been published in the *Journal of the American Ceramic Society* and have been added for purposes normal to dissertation writing.

ABSTRACT

This dissertation represents the culmination of extensive experimentation and research in the area of particulate and whisker reinforced ceramic matrix composites. Diamond, boron carbide, and titanium diboride particles as well as boron carbide whiskers were employed as second phases to improve and enhance the physical properties of the ceramic matrix. Judicious selection of both the toughening agents and the high strength ceramic matrices, as well as the appropriate processing treatment have yielded composite systems distinguished by their outstanding thermal and/or mechanical properties.

The main body of this dissertation is comprised of four papers. Two have been published in the Journal of the American Ceramic Society, while the other two have been published in the Ceramic Engineering Science Proceedings. The Appendices include two other recently published papers which are also part of this dissertation research.

"Particulate and Whisker Reinforced Alumina Matrix Composites" summarizes the interaction of various reinforcing media within an alumina matrix and the resulting effect they impart upon various physical properties. "Normal Pressure Hot Pressing of α -Alumina/Diamond Composites" and "Nano-Diamond Enhanced Silicon Carbide Matrix Composites" discuss the processing of unique high hardness, high thermal performance diamond composites utilizing α -alumina and silicon carbide matrices, respectively. Discussion and assessment of both the whisker and particle effects of boron carbide on the α -alumina matrix is given in "Physical Properties of Alumina-Boron Carbide Whisker/Particle Composites" and in Appendix A, "Boron Carbide Reinforced Ceramic Matrix Composites." In Appendix B, the paper entitled, "Enhanced Mechanical Properties of Alumina by Dispersed Titanium Diboride Particulate Inclusions" examines composites of the α -alumina/titanium diboride particle system and compares various methods of fracture toughness measurement for such composites.

ACKNOWLEDGMENTS

The author wishes to express his most profound gratitude to his advisor, Dr. P.D. Ownby, for his guidance, assistance, and encouragement during his graduate studies. Furthermore, the author would like to acknowledge the financial assistance of MRD Corporation, Dr. P.D. Ownby, and the Department of Ceramic Engineering throughout his term of study at the University of Missouri-Rolla.

In addition, the author extends special thanks to Dr. S.A. Howard, for his expert assistance and insightful direction in the X-ray diffraction phase analysis, as well as to his committee members, Dr. R.E. Moore, Dr. M.N. Rahaman, Dr. R.A. Kohser, and Dr. J.W. Newkirk for their review and criticism of this dissertation.

Finally, the author wishes to bestow his utmost gratitude upon his family for their limitless sacrifice, constant encouragement, and implicit faith, without which this achievement could not have been possible.

TABLE OF CONTENTS

	Page
PUBLICATION DISSERTATION OPTION	iii
ABSTRACT	iv
ACKNOWLEDGMENTS	v
LIST OF ILLUSTRATIONS	x
LIST OF TABLES	xiv
 PAPER 1 -- Particulate and Whisker Reinforced Alumina Matrix	
Composites	1
Abstract	2
I. Introduction	3
(1) Particulate reinforced ceramic matrix composites	5
(A) Residual stress and microcrack toughness enhancing mechanisms	5
(B) Crack deflection mechanism	7
(C) Bridging toughness mechanism	7
(2) Whisker reinforced ceramic matrix composites	8
II. Experimental Procedure	9
III. Results and Discussion	10
(1) Particulate reinforced ceramic matrix composites	10

TABLE OF CONTENTS (Cont.)

	Page
(A) α -alumina matrix composites	11
(B) β^*/β -alumina ceramic matrix composites	11
(2) Whisker reinforced ceramic matrix composites	13
IV. Conclusion	14
References	16
Figure Captions	20
 PAPER 2 -- Normal Pressure Hot Pressing of α -Alumina/Diamond	
Composites	28
Abstract	29
I. Introduction	30
II. Experimental Procedure	31
III. Results and Discussion	32
(1) Density	33
(2) Mechanical properties	33
(3) Thermal expansion coefficients	34
(4) Thermal conductivity and thermal shock resistance	35
IV. Conclusion	35
Acknowledgment	36
References	37
Figure Captions	40

TABLE OF CONTENTS (Cont.)

	Page
PAPER 3 -- Physical Properties of Alumina-Boron Carbide Whisker/Particle	
Composites	47
Abstract	48
I. Introduction	49
II. Materials	50
III. Experimental Procedure	51
IV. Results and Discussion	52
(1) Density	52
(2) Mechanical properties	52
(3) Microstructure	54
(4) Thermal expansion of α -alumina-boron carbide composites	54
References	55
Figure Captions	59
PAPER 4 -- Nano-Diamond Enhanced Silicon Carbide Matrix Composites	64
Abstract	65
I. Introduction	66
II. Experimental Procedure	67
III. Results and Discussion	68

TABLE OF CONTENTS (Cont.)

	Page
(1) Polytypes of diamond and silicon carbide	68
(2) Residual stress	69
(3) Crack deflection by diamond particles	70
(4) Thermal conductivity and thermal shock resistance	70
(5) X-ray analysis	71
(6) Density and Fracture toughness, K_{Ic} ,	72
References	74
Figure Captions	78
VITA	85
APPENDIX A: Boron Carbide Reinforced Ceramic Matrix Composites	86
APPENDIX B: Enhanced Mechanical Properties of Alumina by Dispersed Titanium Dioxide Particulate Inclusions	91

LIST OF ILLUSTRATIONS

Figure	Page
PAPER 1 -- Particulate and Whisker Reinforced Alumina Matrix Composites	
Fig. 1.	Ceramic inclusions used in this investigation.. 21
Fig. 2.	Fracture toughening mechanisms in particulate and whisker reinforced ceramic matrix composites.. 22
Fig. 3.	Flow chart of experimental procedure. 23
Fig. 4.	Fracture toughness measurement techniques. 24
Fig. 5.	Fracture toughness of α -alumina with various second phase additions. 25
Fig. 6.	Fracture toughness of α -alumina and β''/β -alumina reinforced with titanium diboride particle additions. After ²¹ 26
Fig. 7.	Fracture toughness of alumina vs volume percent boron carbide particles and whiskers measured by the CNSR technique. After ²² 27

LIST OF ILLUSTRATIONS (Cont.)

Figure	Page
PAPER 2 -- Normal Pressure Hot Pressing of α-Alumina/Diamond Composites	
Fig. 1.	Scanning electron micrograph of as-received (a) S-diamond 1/2-1 μm particle powder (b) M-diamond 0-5 μm particle powder. 41
Fig. 2.	The X-ray pattern of α -alumina/diamond composites at room temperature. 42
Fig. 3.	Density of α -alumina vs volume percent diamond particles. 43
Fig. 4.	Fracture toughness of α -alumina vs volume percent diamond particles measured by the CNSR technique. 44
Fig. 5.	Diametral tensile strength of α -alumina vs volume percent S-diamond particles. 45
Fig. 6.	Theoretical variation of the thermal conductivity with volume percent diamond particles. 46

LIST OF ILLUSTRATIONS (Cont.)

Figure	Page
PAPER 3 – Physical Properties of Alumina-Boron Carbide Whisker/Particle Composites	
Fig. 1.	Theoretical composite density (%) versus volume percent boron carbide particles and boron carbide whiskers. 59
Fig. 2.	Fracture toughness of alumina versus volume percent boron carbide particles and boron carbide whiskers. 60
Fig. 3.	Flexural strength of alumina versus volume percent boron carbide particles and boron carbide whiskers. 61
Fig. 4.	Scanning electron micrograph of a polished surface of (a) alumina with 15 vol.% boron carbide powder particles (b) alumina with 15 vol.% boron carbide whiskers. 62
Fig. 5.	Scanning electron micrograph of a fracture surface of (a) intergranular fracture of alumina with 15 vol.% boron carbide powder particles (b) whisker pullout of alumina with 15 vol.% boron carbide whiskers. 63

LIST OF ILLUSTRATIONS (Cont.)

Figure	Page
PAPER 4 -- Nano-Diamond Enhanced Silicon Carbide Matrix Composites	
Fig. 1.	Theoretical variation of the thermal conductivity with volume percent diamond. 79
Fig. 2.	The coexistence of Diamond-3C and Diamond-2H of as received 1 μm diamond powder. 80
Fig. 3.	The results of the XRD analysis of a densified silicon carbide - 31% diamond composite specimen. 81
Fig. 4.	Theoretical composite density vs the volume percent of nano-diamond particle addition. 82
Fig. 5.	Fracture toughness, K_{Ic} , of silicon carbide with different volume percents of dispersed 11 nm diamond particles measured by the indentation method with a 30 Kg load. 83
Fig. 6.	Fracture toughness of silicon carbide with 18.5 volume percent of different particle sizes of diamond measured by the indentation method with a 30 Kg load. 84

LIST OF TABLES

Table	Page
PAPER 1 -- Particulate and Whisker Reinforced Alumina Matrix Composites	
Table I Physical Properties of Alumina, Silicon Carbide, Titanium Diboride, Boron Carbide and Diamond ²⁰	19
PAPER 2 -- Normal Pressure Hot Pressing of α -Alumina/Diamond Composites	
Table I Thermal Expansion Coefficients of Alumina/Diamond Composites.	39
PAPER 3 -- Physical Properties of Alumina-Boron Carbide Whisker/Particle Composites	
Table I Thermal Expansion Coefficients of Alumina-Boron Carbide Whisker Composites	57
PAPER 4 -- Nano-Diamond Enhanced Silicon Carbide Matrix Composites	
Table I Polytypes of Diamond and Silicon Carbide ⁺	76
Table II Physical Properties of Polycrystalline Silicon Carbide, Diamond, and Cubic Boron Nitride	77

PAPER 1

Particulate and Whisker Reinforced Alumina Matrix Composites

Jenq Liu* and P. Darrell Ownby*

Ceramic Engineering Department

University of Missouri-Rolla

Rolla, Missouri 65401

*: members, American Ceramic Society

COMISSÃO NACIONAL DE ENERGIA NUCLEAR/SP - FEN

Particulate and Whisker Reinforced Alumina Matrix Composites

Abstract

The fracture toughness of alumina has been successfully improved by adding isolated, titanium diboride, boron carbide, or diamond particles or boron carbide whiskers. Titanium diboride particles yield a higher fracture toughness improvement than boron carbide, or diamond particles in high strength reinforced α -alumina matrix composites even though diamond has a much higher Young's modulus.

For particulate reinforced ceramic matrix composites, a lower thermal expansion coefficient of the second phase can also produce a toughness enhancement. For a second phase to be effective in toughening a high strength ceramic matrix composite, a compressive residual hoop stress is necessary but not sufficient. Whiskers are more effective than more equiaxed particulates for increasing the fracture toughness of a given matrix.

[Key words: Mechanical properties, Diamond, Boron carbide particles, Titanium diboride whiskers, Alumina, Composites]

I. Introduction

The physical properties of ceramics can be enhanced by adding a second phase. The second phase may be either metallic or ceramic. Metal reinforced ceramic matrix composites which exhibit a high fracture toughness, include WC/Co¹, Al₂O₃/Al², B₄C/Al,³ and SiC/Al⁴ composites. The relatively low Young's modulus, and strength and higher fracture toughness of the metal second phase, which usually has a lower melting temperature, will often form a solid solution phase with the matrix which coexists at the metal ceramic interface in the composites. This solid solution phase usually increases the bonding between the metal second phase and the ceramic matrix, and decreases the sintering temperature. The fracture toughness is often increased by the metal ligament bridging effect.⁴ This well-bonded interface and liquid phase sintering mechanism in metal reinforced composites is different from brittle ceramic reinforced ceramic matrix composites.

Ceramic reinforced ceramic matrix composites benefit from different toughening mechanisms than ceramic-metal composites. The ceramic reinforced composites can be divided into three groups according to the stability of the second phase as shown in Fig. 1. The first group is characterized by a stable non-reacted second phase such as a ceramic particle, whisker, or fiber reinforced ceramic.⁵ The second group depends on a ceramic crystallographic phase transformation of the second phase yielding transformation toughened ceramics.⁶ The third group includes an unstable reacted second phase. Second phase composites from the first group only are included in this study.

A high Young's modulus, high strength, non-reactive ceramic second phase and the ceramic matrix constitute composites with uniquely improved mechanical properties. The dominant fracture toughness enhancing factors are related to the nature of the interface between the second phase and matrix and the differences between the physical properties of the two phases. The interfacial characteristics are determined by the inherent physical properties of each of the two phases, and their chemical bonding and stability in contact. Interfaces are also characterized by the interfacial roughness, chemical homogeneity, etc, which may be determined by the processing techniques. Chemical stability of the two phases is a major concern in selecting the toughening reinforcement second phase. Other factors, such as, the occurrence of wetting, which will form a well bonded interface, are also considered. The important physical property differences include thermal expansion mismatch, and Young's modulus mismatch which will caused a residual stress to develop and consequently a stress concentration at the interface of the second phase and the matrix.

The ceramic second-phase can be in the form of either particles, whiskers or fibers. Particle and whisker containing composites are easier to fabricate than continuous fiber composites, but have less specific directional control of the improvement in the mechanical properties. Particle containing composites have the most isotropic properties and are easiest to prepare. Whisker containing composites have the highest strength because of the inherent strength of single crystal whiskers which approach the theoretical strength value. The single most significant feature of non-reacted two phase composites is the increase in fracture toughness over that inherent in the matrix. These high fracture

toughness composites tend to prevent catastrophic failure. This increase can be expressed in terms of either the change in the critical stress intensity factor, K_{Ic}^7 , or the critical strain energy release rate ΔG_c^8 .

$$\Delta K_{Ic} = -\left(\frac{2}{\pi}\right)^{1/2} f^0 \int_0^l \frac{\sigma(x)}{x^{1/2}} dx \quad (1)$$

where f is the area fraction of reinforcement along the crack plane, σ is the normal stress on the reinforcement between the crack surface, and x is the distance from the crack tip.

$$\Delta G_c = 2f^0 \int_0^u \sigma(u) du \quad (2)$$

where u is the crack opening at the end of the bridging zone.

The mechanisms for increasing the fracture toughness by non-reacted particles, or whisker reinforced ceramics are determined by the interactions between the second phase - matrix interface and a propagating crack as shown in Fig. 2. These interaction mechanisms include crack deflection⁹, sub-critical microcracking^{10,11}, crack bridging^{4,12}, and residual stress¹³, which are discussed in the following sections.

(1) *Particulate reinforced ceramic matrix composites*

(A) *Residual stress and microcrack toughness enhancing mechanisms:* The difference in thermal expansion coefficient, α , and Young's modulus between the second phase and the matrix result in the formation of residual stress in the particles and surrounding matrix during cooling after fabrication. This stress may cause crack travel around the

particle, or may cause sub-critical microcracks which reinforce the matrix.

(i). if $\alpha_p > \alpha_m$, upon cooling the matrix develops radial tension and tangential hoop compressive stress, whereas the second phase particle is under tension, and tension is generated at the interface. Matrix precompressing by the second phase could result in crack travel around the second phase. If the second phase particle is near the plane of a crack, the crack should be first deflected to the particle plane as it approaches the particle and then move around it. When a crack tip reaches a position above the particle it will be oriented normal to the radial tensile stress axis and can be deflected back to the particle-matrix interface.

(ii) if $\alpha_p < \alpha_m$, upon cooling, the matrix is under tangential hoop tension and the second phase particle is under compression. A crack is then attracted to the second phase. Interfacial compressive stresses are also created, which increase the effective shear resistance of the second phase/matrix interface. The hoop tensile stresses which develop may provide matrix microcracking.

Analysis of these residual stresses, the radial matrix stress (σ_{mr}) and the tangential matrix stress ($-2\sigma_{m\theta} = \sigma_{m\tau}$) is based on the hydrostatic stress (σ_h) developed around the particle. For spherical particles, the hydrostatic stress can be calculated by the following equation¹⁴:

$$q = \sigma_{r\tau} = \sigma_h = \frac{(\alpha_p - \alpha_m)\Delta T}{\left[\frac{(1 + \nu_m)}{2E_m}\right] + \left[\frac{(1 - 2\nu_p)}{E_p}\right]} \quad (3)$$

where α is the thermal expansion coefficient, E is Young's modulus, ν is poisson's ratio,

and ΔT is the temperature range over which stresses are not relieved by diffusive processes.

The fracture toughness increase by the residual stress effect can be estimated by the following equation¹² as:

$$\Delta K_{Ic} = 2q \left(\frac{2D}{\pi} \right)^{1/2} \quad (4)$$

where q is the local residual stress, and D is the length of the stress zone.

To increase the fracture toughness a $\alpha_p > \alpha_m$ is essential to create crack travel around the second phase particles.

(B) Crack deflection mechanism: For crack deflection to occur a strong, high Young's modulus second phase particle is necessary to deflect the propagating crack and to generate a non-planar crack. A strong interface is necessary to transfer the crack-load. A $\alpha_p < \alpha_m$ is essential to create crack travel to the second phase particles, which will twist or tilt the crack path. The crack deflection mechanism depends on the volume % of the second phase volume % and shape of the second phase but is independent of the second phase particle size. This mechanism usually combines with residual stress to increase the fracture toughness of the matrix. Such composites include glasses reinforced with silicon carbide, and/or silicon nitride⁹, and silicon carbide-titanium diboride¹⁵ and, alumina-titanium carbide¹⁶ composites.

(C) Bridging toughness mechanism: A low fracture toughness second phase can also increase the composite mechanical properties by crack bridging effects. Bridges occur when a weak interface is generated by the non-reaction between the particle and matrix

or at the grain boundary. A crack will travel and be deflected along the interface, which poses a low fracture energy, and particle ligaments will be produced behind the crack front. Such composites include alumina and silicon nitride reinforced with silicon carbide particles.

(2) Whisker reinforced ceramic matrix composites

The fracture toughness mechanisms of whisker reinforced composites are basically similar to that of particle reinforced composites. The crack deflection mechanism is increased because of the high aspect ratio of a whisker, and residual stress toughness mechanisms will be overcome by other mechanisms. Bridging effects are prominent factors for brittle ceramic reinforced composites. Bridging effects depend on the nature of the interface between the whisker and the matrix. A weak interface is required to increase the debonding or the pull-out length.¹⁷ This mechanism requires second phase whiskers with a high transverse fracture toughness relative to the interfacial fracture toughness so that failure occurs first along the whisker-matrix interface. Toughening results from the additional work required when whiskers pull-out by debonding behind the crack tip. The stresses transferred to the whisker must be less than the fracture strength of the whisker, but the interfacial shear stress generated must be greater than the shear resistance of the whisker/matrix interface. The shear resistance is controlled by the degree of chemical and/or mechanical bonding between the whisker and the matrix. Thus the interfacial shear resistance between the whisker and the matrix is important in determining the preferred fracture paths and ultimately whisker debonding and pull-out.

The toughness effect generated by whisker additions can be expressed by the fracture toughness increase and the strain energy release rate. The fracture toughness increase is based on the critical stress intensity factor term and can be estimated by the equation derived by Becher et.al.¹² as shown in the following equation.

$$\Delta K_{Ic} = \sigma_f \left[\frac{V_f^w r E^c G^w}{6(1-\nu^2) E^w G^i} \right]^{1/2} \quad (5)$$

Where V_f is the whisker volume fraction, E is Young's modulus, ν is poisson's ratio, r is the whisker radius, G is the strain energy release rate, and subscripts w stands for whisker, c for composite, and i for interface.

The strain energy release rate can be estimated by the equation derived by Evans et.al.⁵

$$\Delta G_c = fd[S^2/E - E(\epsilon_{ij}^T)^2 + 4\Gamma/R(1-f)] + 2\tau fh_p^2/R \quad (6)$$

where d is the debonding length, S is the whisker length, ϵ is the stress free strain, Γ is the fracture energy of the interface, τ is the shear resistance of the interface after debonding, R is the whisker radius, and h_p is the whisker pullout length.

II. Experimental Procedure

The matrices chosen in this study were high strength α -alumina and relatively lower strength β "/ β -alumina. Diamond, boron carbide, and titanium diboride particles were used as the toughness reinforcement materials. Boron carbide single crystal whiskers were used to study the effects of whiskers in contrast to particles. Each one of the

materials has a different strength, Young's modulus, and thermal expansion coefficient. The physical properties of each are listed in Table I. The flow chart of the experimental procedure is shown in Fig. 3.

The as-received powders were first analyzed by Horiba* particle size analysis to determine their particle size distribution and then further examined by Scanning Electron Microscopy (SEM) to characterize their shape and size.

These second phase particles were wet mixed with alumina matrix powders, and then oven dried. The mixed and granulated powders were then hot pressed to a desired dimension and density for mechanical property tests. The Chevron Notch Short Rod, CNSR,** Direct Crack Measurement, DCM, and Single Edge Notch Beam, SENB techniques as shown in Fig. 4. were used to measure the composite fracture toughness^{18,19}.

III. Results and Discussion

(1) *Particulate reinforced ceramic matrix composites*

Multiple toughness mechanisms are responsible for enhancing the toughness and therefore it is difficult to determine one solitary dominant mechanism. These multiple factors such as crack deflection, crack bridging, residual stress and microcracking are referred to generally as crack interactions between particles and the ceramic matrix.

* Horiba CCAPA-700, Horiba, Ltd.

** Fractometer I, Terra Tek systems, Inc. Salt lake City, Utah.

The fracture toughness of the ceramic matrix is increased with second phase particle additions, regardless of the sign of the hoop stress in the matrix, *i.e.* it may be in tension or compression as shown in Figs. 5 and 6. Compressive residual stress is not an essential factor in increasing the fracture toughness for high strength alumina ceramic matrix systems, although the fracture toughness increase is higher for the compressive residual stress developed composites. These results are contrary to those expressed by equation (4), which requires that compressive hoop stress will increase the fracture toughness, and tensile hoop stress will decrease the fracture toughness.

To illustrate, for the same α -alumina matrix, the hoop tensile residual stress developed by the three different composites is calculated as described in equation (3).

(A) α -alumina matrix composites:

α -alumina-diamond composite, $\alpha_p < \alpha_m$

$$-2\sigma_{m\theta} = \sigma_{mr} = \sigma_n = (3.9-8.6)10^{-6} \cdot 1000 / [(1+0.26)/2 \cdot 380 \text{ GPa}] + [1-(2 \cdot 0.20)/925 \text{ GPa}]$$

$$\sigma_{m\theta} = 1020 \text{ MPa.}$$

α -alumina-boron carbide composite, $\alpha_p < \alpha_m$

$$-2\sigma_{m\theta} = \sigma_{mr} = \sigma_n = (5.0-8.6)10^{-6} \cdot 1000 / [(1+0.26)/2 \cdot 380 \text{ GPa}] + [1-(2 \cdot 0.17)/450 \text{ GPa}]$$

$$\sigma_{m\theta} = 576 \text{ MPa.}$$

α -alumina-titanium diboride composite, $\alpha_p < \alpha_m$

$$-2\sigma_{m\theta} = \sigma_{mr} = \sigma_n = (8.1-8.6)10^{-6} \cdot 1000 / [(1+0.26)/2 \cdot 380 \text{ GPa}] + [1-(2 \cdot 0.28)/574 \text{ GPa.}]$$

$$\sigma_{m\theta} = 103 \text{ MPa.}$$

(B) β^*/β -alumina ceramic matrix composites:

β^*/β -alumina-titanium diboride composite, $\alpha_p > \alpha_m$,

The compressive residual hoop stress is created surrounding the particle in the β''/β -alumina matrix and is calculated as follows:

$$-2\sigma_{\text{res}} = \sigma_{\text{int}} = \sigma_{\text{a}} = (7.8-8.1)10^{-6} \cdot 1000 / [(1+0.26)/2 \cdot 210 \text{ GPa}] + [1-(2 \cdot 0.25)/574 \text{ GPa}]$$

$$\sigma_{\text{res}} = -39 \text{ MPa.}$$

By comparing the resulting toughness increases produced by these different residual stresses, it is revealed that the titanium diboride reinforced alumina matrix composites have lower interfacial stresses but a higher fracture toughness increase. It is also noted that the fracture toughness enhancement occurs in both hoop compressive stress and hoop tensile stress situations. The α -alumina/titanium diboride composites produce a tensile residual hoop stress (103 MPa) and β''/β -alumina/titanium diboride composites produced a compressive residual hoop stress (-39 MPa). The fracture toughness improvement, (K_{IC} composite/ K_{IC} matrix) in the β''/β -alumina matrix is 2.1 which is higher than the 1.65 for the α -alumina matrix as shown in the Fig. 6. These two composites had almost the same matrix grain size distribution (1-2 μm), thus the grain size considerations can be eliminated in both composites.

Other reinforcement materials with a large negative thermal expansion coefficient mismatch, such as boron carbide and diamond, will also generate a high hoop tensile stress. The fracture toughness enhancement for the composites is lower than α -alumina/titanium diboride but it does not have a decreasing fracture toughness as predicted by equation (4).

For α -alumina matrix composites, all three of the cited second phases possess a thermal expansion coefficient smaller than α -alumina, thus a residual tensile stress is

developed. This tensile stress attracts the crack toward the second phase particles. To increase the fracture toughness, the second phase must itself have a high fracture toughness and/or high strength to deflect the crack, such as in the case of titanium diboride, boron carbide or diamond, or have low interfacial stress to provide a grain bridge. However, a very high Young's modulus, and very strong second phase (a very large difference in Young's Modulus) particle, such as diamond, is not a necessary but a sufficient factor to deflect the propagating crack in particle reinforced ceramic matrix composites. When a residual tensile stress is developed, a higher Young's modulus, and higher strength in the second phase particles assists the deflection of the crack, and increases the toughness, but a very large difference in Young's modulus and strength will increase the hoop tensile stress, which may decrease the fracture toughness.

It is, therefore suggested that the fracture toughness enhancement of alumina ceramic matrix composites by the addition of a stronger second phase hard particle is a result of a combination of factors, namely, grain bridging, crack deflection, residual stress and microcracking. Compressive hoop stress (positive thermal expansion coefficient mismatch) will contribute to the increased fracture toughness, but the decreased fracture toughness by tensile hoop stress (negative thermal expansion coefficient mismatch) will be overcome by the fracture toughness increase caused by bridging and crack deflection.

(2) Whisker reinforced ceramic matrix composites

The fracture toughness, K_{Ic} , of α -alumina as a function of volume percent boron carbide whiskers is presented graphically in Fig. 7. Boron carbide whiskers have a

significant effect on increasing the fracture toughness. When comparing these results with particle reinforced alumina matrix composites we observed several things:

- (i). The fracture toughness of the alumina matrix is increased linearly with the second phase whisker additions up to a certain vol. %.
- (ii). Whiskers enhance the fracture toughness better than particles of the same composition in the same matrix as shown in Fig. 7.
- (iii). Single crystal boron carbide whiskers have high strength, and low fracture toughness compared to the α -alumina matrix. This indicates that the strength of the whisker is one of the determining factors in the toughness enhancing mechanism as is the case in alumina-silicon carbide whisker composites¹².
- (iv) The large aspect ratio, and the weak interface encountered by the crack promotes the probability of the bridging effect.

IV. Conclusion

Enhanced toughness, may occur by more than one mechanism. The dominant mechanism is not the same for particulate and whisker reinforced ceramic matrix composites. For particulate reinforced ceramic matrix composites, a lower thermal expansion coefficient of the second phase can produce a toughness enhancement.

In choosing a second phase for a high strength ceramic matrix, a compressive residual hoop stress is necessary but not sufficient. When a tensile residual hoop stress is generated, a high Young's modulus and high strength of a second phase is needed to

deflect a propagating crack, but this Young's modulus should not generate a very high tensile hoop stress, which may decrease the fracture toughness. However, when a compressive residual hoop stress is generated, a high Young's modulus and high strength of second phase is necessary to further increase the fracture toughness.

For an α -alumina matrix, we found that the titanium diboride particle is more effective in increasing the toughness and strength of an alumina matrix than boron carbide, or diamond particles, although the diamond particle has an extremely high Young's modulus. Since the titanium diboride particle has a similar thermal expansion coefficient, it will generate a smaller interfacial stress than a boron carbide or diamond particle in α -alumina composites. Furthermore titanium diboride particles are more thermally stable than diamond, or boron carbide particles. However, when combining fracture toughness qualities with other physical properties, such as thermal conductivity or wear resistance, diamond should be considered as a prime particle reinforcement candidate.

Whiskers are more effective than more equiaxed particulates for increasing the fracture toughness of the same matrix.

References

1. D.B. Marshall, W.L. Morris, B.N. Cox, and M. S. Dadkhah, "Toughening Mechanism in Cemented Carbides," *J. Am. Ceram. Soc.*, **73** [10] 2938-43 (1990).
2. E. Breval, M.K. Aghajanian, and S.J. Luszcz, "Microstructure and Composition of Alumina/Aluminum Composites Made by Directed Oxidation of Aluminum," *J. Am. Ceram. Soc.*, **73** [9] 2610-14 (1990).
3. D.C. Halverson, A.J. Pyzik, I.A. Aksay, and W.E. Snowden, "Processing of Boron Carbide-Aluminum Composites," *J. Am. Ceram. Soc.*, **72** [5] 775-80 (1989).
4. B. Budiansky, J.C. Amazigo, and A.G. Evans "Small-Scale Crack Bridging and the Fracture Toughness of Particulate-Reinforced Ceramics," *J. Mech. Phys. Solid.*, **36** [2]167-87 (1988).
5. A.G. Evans "Perspective on the Development of High-Toughness Ceramics," *J. Am. Ceram. Soc.*, **73** [2] 187-206(1990).
6. A.G. Evans and R.M. Cannon, "Toughening of Brittle Solids by Martensite Transformations," *Acta Metall.*, **34** [5] 761-800 (1986).
7. G.C. Sih, Handbook of Stress Intensity Factors. Lehigh Univ. Press.
8. R.W. Rice, "Mechanisms of Toughness in Ceramic Matrix Composite," *Ceram. Eng. Sci. Pro.*, **2** [7-8] 661-701 (1981).
9. K.T. Faber and A.G. Evans, "Crack Deflection Processes-I. Theory," *Acta Metall.*, **31** [4] 565-76 (1983).

10. Y. Fu and A.G. Evans, "Some Effects of Microcracks on the Mechanical Properties of Brittle Solids-I. Stress, Strain Relations," *Acta Metall.*, 33 [8] 1515-23 (1985).
11. Y.Fu, and A. G. Evans, "Some Effects of Microcracks on the Mechanical Properties of Brittle Solids-II Microcrack Toughening," *Acta Metall.*, 33 [8] 1525-31 (1985).
12. P.F. Becher, C. Hsueh, P. Angelini and T.N. Tieggs, "Toughening Behavior in Whisker-Reinforced Ceramic Matrix Composites," *J. Am. Ceram. Soc.*, 71 [12] 1050-1061 (1989).
13. M. Taya, S.Hayashi, A.S. Kobayashi, and H.S. Yoon, "Toughening of a Particulate-Reinforced Ceramic-Matrix Composite by Thermal Residual Stress," *J. Am. Ceram. Soc.*, 73[5] 1382-91 (1990).
14. J. Selsing, "Internal Stresses in Ceramics," *J. Am. Ceram. Soc.*, 44 [8] 419 (1961).
15. C.H. McMurtry, W.D.G. Boecker, S.G. Seshadri, and J.S. Zanghi, "Microstructure and Material Properties of SiC-TiB₂ Particulate Composite," *Am. Ceram. Soc. Bull.*, 66 [2] 325-29 (1987).
16. R.P. Wahi and B. Ilshner, "Fracture Behaviour of Composites Based on Al₂O₃-TiC," *J. Mater. Sci.*, 15, 875-85 (1980).
17. A.G. Evans and M.Y. He, "Interface Debonding and Fiber Cracking in Brittle Matrix Composites," *J. Am. Ceram. Soc.*, 72 [12] 2300-303 (1989).

18. J. Liu and P.D. Ownby, "Enhanced Mechanical Properties of Alumina by Titanium Diboride Particulate Inclusions," *J. Am. Ceram. Soc.*, **73** [1] 241-43 (1991).
19. L.M. Barker, "Short Bar Specimens for (K_{Ic}) Measurements"; pp. 73-82 in *Fracture Mechanics Applied to Brittle Materials*, ASTM STP 678. Edited by S. W. Freiman. American Society for Testing and Materials, Philadelphia, PA, 1979.
20. W.J. Lackey, D.P. Stinton, G.A. Cerny, A.C. Schaffhauser, and L.L. Fehrenbacher, "Ceramic Coatings for Advanced Heat Engines-A Review and Projection," *Adv. Ceram. Mat.*, **2** [1] 24-30 (1987).
21. J. Liu, and P.D. Ownby, "Boron Containing Ceramic Particulate and Whisker Enhancement of the Fracture Toughness of Ceramic Matrix", Proceedings of the 10th International Symposium on Boron, Borides, and Related Compounds, (Albuquerque, NM. August 27-30, 1990). Edited by D. Emin and T. Aselage. American Institute of Physics, New York, 1991.
22. J. Liu and P.D. Ownby, "Boron Carbide Reinforced Alumina Composites," *J. Am. Ceram. Soc.*, **74** [3] 674-676 (1991).

Table 1. Physical Properties of Alumina, Silicon Carbide, Titanium Diboride, Boron Carbide, and Diamond²⁰

Material	Theor. Density g/cc	Young's Modulus GPa.	Poisson's Ratio	Thermal Expansion $\times 10^{-6}/K$	Vicker or Knoop Hardness GPa.	Transverse Rupture Strength MPa.	Fracture Toughness K_{Ic} MPa.m ^{1/2}
β -alumina	3.28	210	0.25	7.8	13	230-330	2.7
α -alumina	3.98	380	0.26	7.2-8.6	18-23	276-1034	2.7-4.2
silicon carbide	3.21	207-440	0.19	4.3-5.6	20-30	500-930	3.5-4.0
titanium diboride	4.52	514-574	0.09-0.28	8.1	15-36	700-1000	6.0-8.0
boron carbide	2.51	450	0.17	5.0	30-38	300-500	3.8
diamond	3.52	800-925	0.20	1.3-3.9	35-50	850-1550	6.9-3.4

Figure Captions

- Fig. 1.** Ceramic inclusions used in this investigation.
- Fig. 2.** Fracture toughening mechanisms in particulate and whisker reinforced ceramic matrix composites.
- Fig. 3.** Flow chart of the experimental procedure.
- Fig. 4.** Fracture toughness measurement techniques.
- Fig. 5.** Fracture toughness of α -alumina with various second phase particle additions.
- Fig. 6.** Fracture toughness of α -alumina and β''/β -alumina reinforced with titanium diboride particle additions. After²¹
- Fig. 7.** Fracture toughness of alumina vs volume percent boron carbide particles and whiskers measured by the CNSR technique. After²²

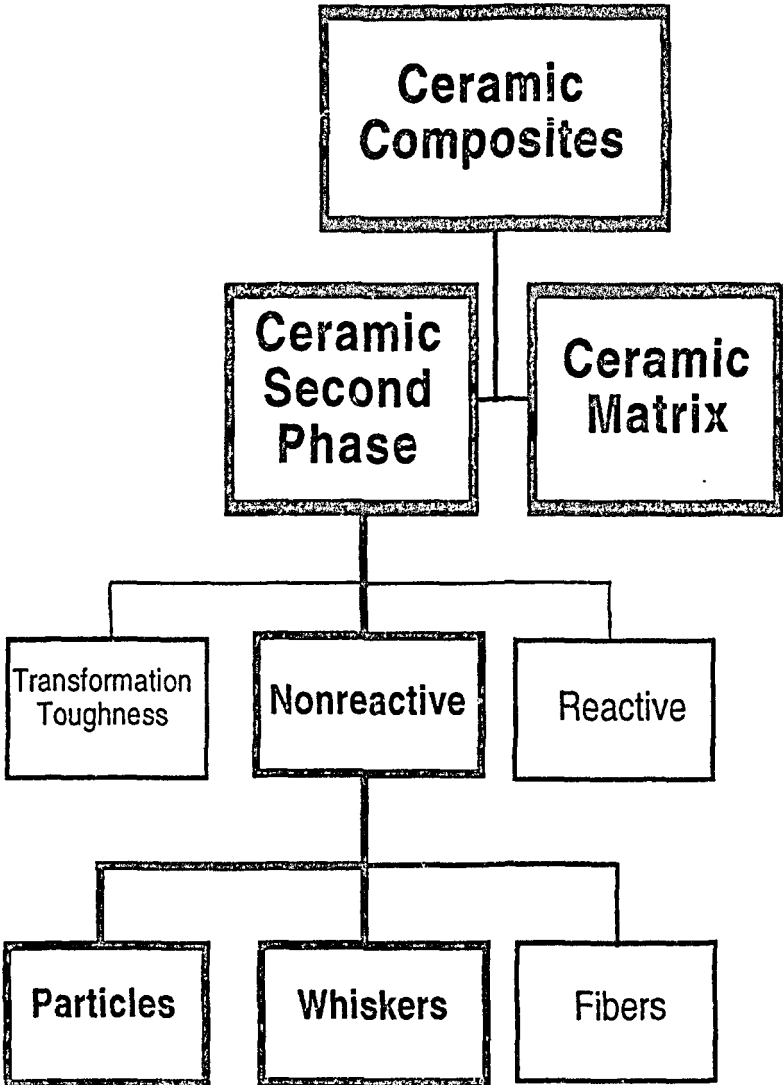


Fig. 1. Ceramic inclusions used in this investigation.

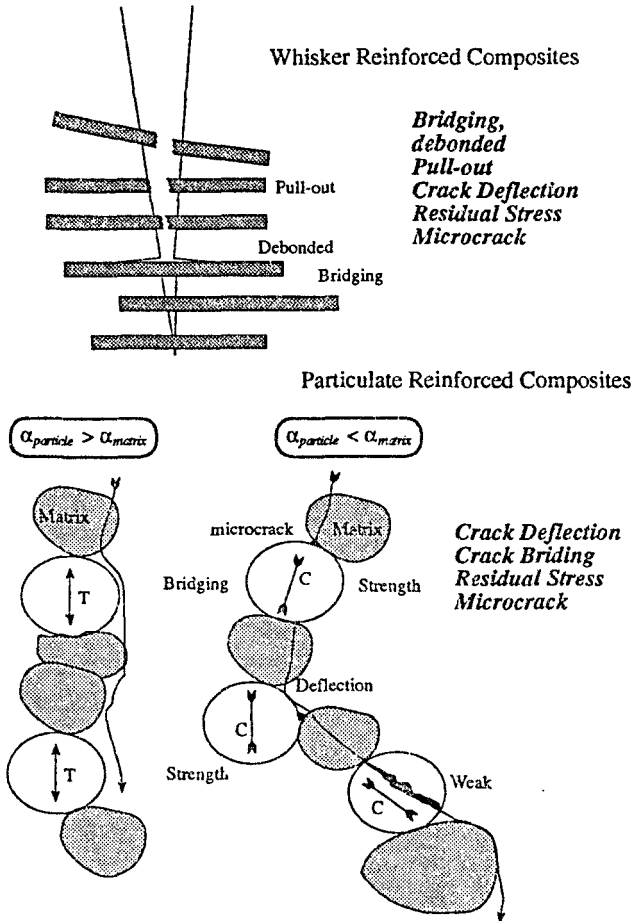


Fig. 2. Fracture toughening mechanisms in particulate and whisker reinforced ceramic matrix composites.

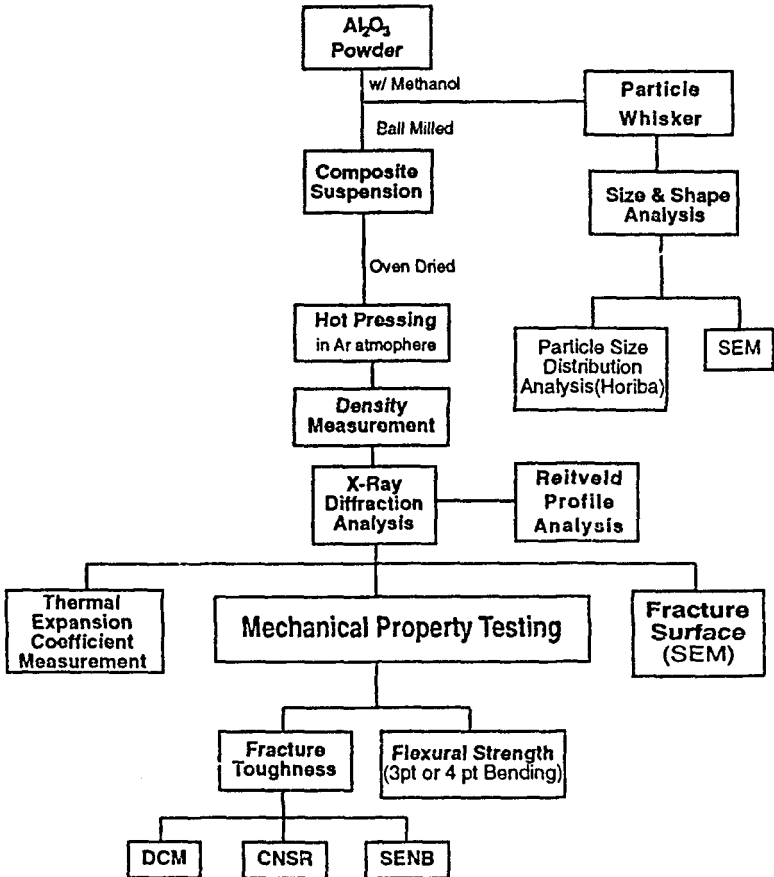
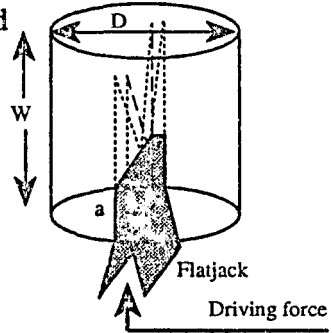


Fig. 3. Flow chart of the experimental procedure.

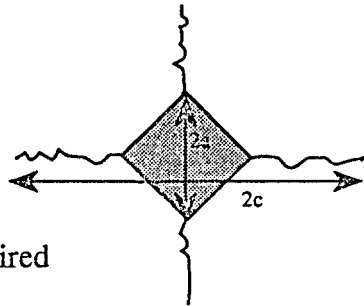
- **CNSR** - small specimen
 - controlled crack growth
 - 0.001" tolerance required

$$\begin{aligned}
 W &= 0.563 \pm 0.02 \text{ in} \\
 D &= 0.375 \pm 0.01 \text{ in} \\
 a &= 0.199 \pm 0.02 \text{ in}
 \end{aligned}$$



- **DCM** - small specimen
 - results vary with different equations
 - low accuracy

$$K_{Ic} = 0.016 \left(\frac{E}{H}\right)^{\frac{1}{2}} \frac{P}{c^{\frac{3}{2}}}$$



- **SENB** - large specimen required

$$K_{Ic} = \frac{3FL}{2bd^2} c^{\frac{1}{2}} y(x)$$

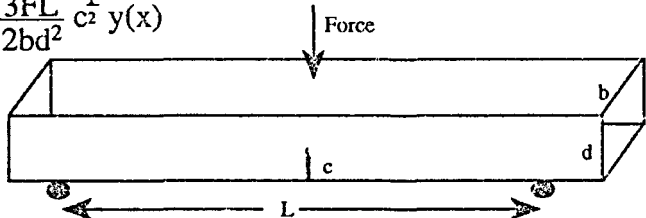


Fig. 4. Fracture toughness measurement techniques.

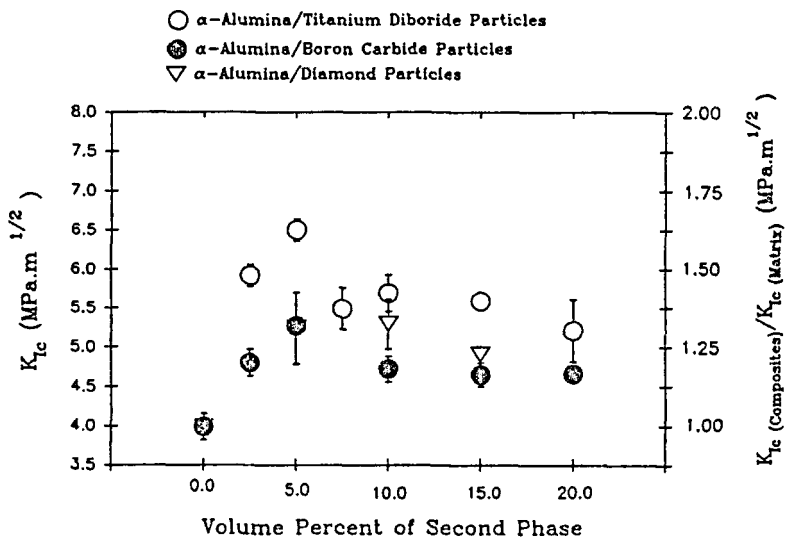


Fig. 5. Fracture toughness of α -alumina with various second phase particle additions.

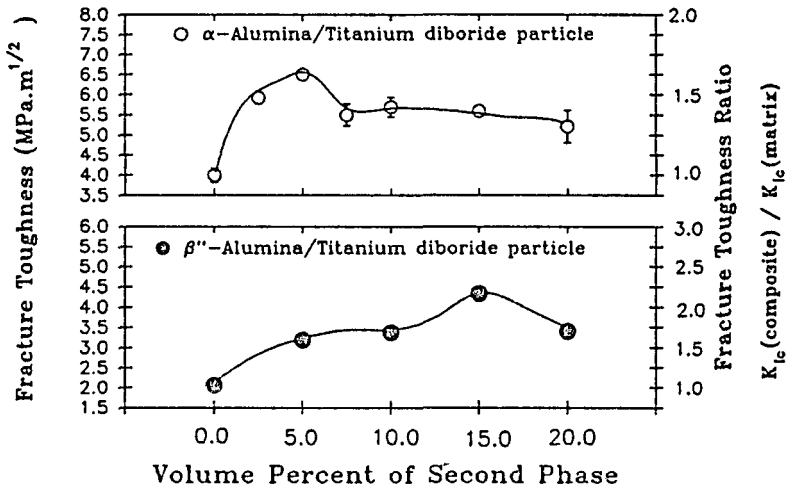


Fig. 6. Fracture toughness of α -alumina and β''/β -alumina reinforced with titanium diboride particle additions. After ²¹

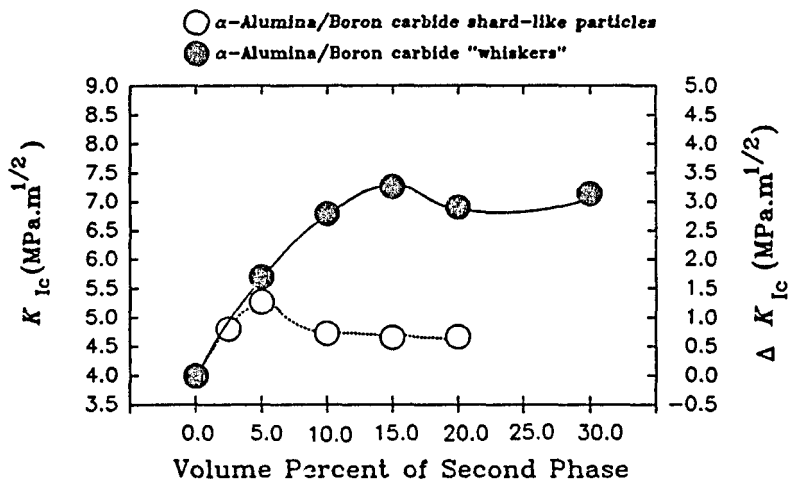


Fig. 7. Fracture toughness of alumina vs volume percent boron carbide particles and whiskers measured by the CNSR technique. After ²²

PAPER 2

Normal Pressure Hot Pressing of α -Alumina/Diamond Composites

J. Liu* and P.D. Ownby*

Department of Ceramic Engineering

University of Missouri-Rolla

Rolla, Missouri 65401

*: members, American Ceramic Society

Normal Pressure Hot Pressing of α -Alumina/Diamond Composites

Abstract

α -alumina/diamond composites have been developed by normal hot pressing procedures using conventional pressure of 32 MPa. and 1250°C. Heretofore this type of composite has required pressure of 60 Kbar to prevent the transformation of diamond to graphite. The mechanical properties, density, and thermal expansion coefficient of these composites have been characterized. The fracture toughness, K_{Ic} , of alumina shows a considerable increase with the addition of diamond particles. Diamond additions tend to decrease the thermal expansion coefficient of these composites. The composite properties are dependent on the volume fraction of diamond particles.

[Key words: Diamond, Alumina, Composites, Thermal expansion coefficient, Fracture toughness.]

I. Introduction

It is well known that a ceramic matrix can be significantly improved in its physical properties by the incorporation of second phase particles^{1,2,3,4}. Diamond is in many respects the ideal "particle", since diamond possesses several unique properties, such as the highest mechanical properties (Young's modulus, strength, and hardness) and an extremely high thermal conductivity.^{6,7,8} These distinctive properties make diamond a preeminent material in several areas, such as those requiring high wear resistance and high thermal conductivity. Diamond has a very high chemical stability at room temperature, however, two of its characteristics, namely oxidation and phase transformation to graphite, have precluded its use as a second phase in ceramic matrix composites produced by conventional fabrication techniques. In order to prevent graphitization, non-conventional processing techniques have been required to produce diamond reinforced ceramic matrix composites. For example, monolithic ceramic-diamond composites have been made experimentally by very high pressure, 60 Kb, high temperature compaction, including silicon carbide-diamond,⁹ alumina-diamond,^{10,11} silicon nitride-diamond¹², and zinc sulfide-diamond¹³ composites. These monolithic composites possess unique mechanical, and thermal properties. Nevertheless, these very-high pressure hot pressed composites are costly and greatly limited in size and shape. A low cost, conventionally processed ceramic-diamond composite is desirable to utilize the unique properties of diamond in practical ceramic applications.

Hot pressed alumina-diamond monolithic composites were produced in this study

utilizing normal hot pressing pressures, with the diamond structure being retained without reaction or graphitization. The mechanical properties and thermal expansion coefficient of the monolithic composites were investigated and are reported.

II. Experimental Procedure

Two different sizes of equiaxed diamond* powder, S-diamond, and M-diamond were used to study the particle size effects on the composite properties. Horiba** particle size analysis determined that the S-diamond powder had a particle size range from $0.05 \mu\text{m}$ - $1 \mu\text{m}$ and an average particle size of $0.48 \mu\text{m}$, which is close the particle size of the alumina matrix. M-diamond powder was found to range from $0 \mu\text{m}$ - $5 \mu\text{m}$ with an average particle size of $1.56 \mu\text{m}$. The as-received diamond powders were then examined by scanning electron microscopy (SEM) to further characterize their shape and size as shown in Fig. 1. Two different types of α -alumina powder were used for the composite matrix, A16SG α -alumina powder,*** with an average particle size of $0.83 \mu\text{m}$, and AKP50 α -alumina**** with an average particle size of $0.33 \mu\text{m}$. Various volume percents of diamond powder were mixed with α -alumina and ball milled in methanol for 2 hours using alumina balls in a plastic jar. The resulting slurries were

* Smith Mega diamond Inc., Provo, UT.

** Horiba CCAPA-700, Horiba, Ltd., Kyoto, Japan

*** ALCOA-A16SG, Alcoa Industrial Chemicals, Bauxite, AR.

**** AKP50, Sumitomo Chemical America, New York, NY.

oven dried. The alumina-diamond granulated powders were hot pressed in BN-coated graphite dies at 32 MPa. and 1250 °C in an argon atmosphere, to achieve a high composite density and prevent oxidation of the diamond. The hot pressed composite specimens were characterized by density, phase content, microstructure, fracture toughness, tensile strength and thermal expansion coefficient, and a theoretical estimate of the thermal conductivity was made. The density was measured by the Archimedes method. The fracture toughness was measured by the CNSR method,¹⁴ the details of which have been described previously⁴. The tensile strength was measured by the indirect diametral compression method¹⁵.

The microstructure of the fracture surfaces were examined by SEM. Precise phase content analysis was accomplished by Rietveld powder X-ray diffraction profile fitting¹⁶.

III. Results and Discussion

Maintaining thermal stability of the diamond structure was critical for this study, since diamond readily transforms to graphite at high temperatures. The graphitization of diamond depends on several factors such as; pressure, temperature, oxygen partial pressure, particle size and the diamond polytype⁹. The normal graphitization of natural diamond occurs from 600-800°C in an oxygen atmosphere,^{6,7,8} however, the graphitization temperature is increased to 1400-1700°C in low oxygen partial pressure⁶. High pressure and smaller surface area (larger particle size) of diamond can also increase

the graphitization temperature.

Chemical stability of the diamond in the α -alumina matrix after hot pressing was confirmed by powder X-ray diffraction which detected no chemical reaction between α -alumina and diamond under these experimental conditions. Furthermore no graphite was detected by Rietveld powder X-ray diffraction profile fitting analysis. A limited 2 theta scan range from the Rietveld profile analysis is shown in Fig. 2. This analysis determined that the 90 volume percent α -alumina, 10 volume percent diamond composites after hot pressing contain 10.4 volume percent diamond with a 1σ (one standard deviation) of 0.5 volume percent. The thermodynamic and chemical stability of diamond in the α -alumina matrix allows these hard, high Young's modulus, high strength particles to provide improved fracture toughness, a lower thermal expansion coefficient, and a higher thermal conductivity for the composites.

(1) Density

The measured hot pressed composite density exhibited a considerable dependence on the volume percent of diamond as shown in the Fig. 3. This trend is the same for both types of α -alumina, but the diamond particle size has no observable effect on the hot pressed composite density.

(2) Mechanical properties

The fracture toughness versus volume percent diamond is presented graphically in Fig. 4. The fracture toughness, K_{Ic} , of α -alumina/diamond composites shows a

considerably higher value than the inherent α -alumina matrix. This increase of the composite fracture toughness is close to other hard particle reinforced alumina matrix composites as presented in previous studies^{4,5}. The fracture toughness of α -alumina/diamond composites was nearly independent of the type of α -alumina powder used.

The operative toughening mechanisms are considered to be related to crack interactions with the diamond hard particles. These interactions may include crack deflection, and crack bridging, with associated stress redistribution at the crack tip when the particles are encountered. Other mechanisms such as subcritical micro-cracks, and crack branching around the diamond particles, are also possible contributors to the significant increase in fracture toughness.

The decreasing tensile strength of α -alumina with various volume percents of diamond particles is shown in Fig. 5. This decreasing strength is opposite to what is found in other alumina matrix composites with second phase particle inclusions which have been shown to exhibit increased strength. This strength drop-off appears to follow the density drop.

(3) Thermal expansion coefficients

Diamond has a low thermal expansion and high thermal conductivity. Therefore diamond addition tends to decrease the thermal expansion coefficient of these composites. The results measured between 100 and 800°C are shown in the Table I, together with the thermal expansion coefficient of diamond itself. They demonstrate that diamond can play

a significant role in decreasing the thermal expansion coefficient of composites.

(4) *Thermal conductivity and thermal shock resistance*

Diamond has an extremely high thermal conductivity, (500-2000 W/m°C)^{6,7,8}, which is higher than copper and silver at room temperature. Alumina, on the other hand is a thermal insulator (27.2 W/m°C)¹⁷. Therefore, consideration of the increase in the thermal conductivity of these composites is appropriate. Such consideration of silicon carbide has been discussed previously¹⁸. The thermal shock resistance of composites containing diamond is also expected to be enhanced. The following treatment displays the expected results according to Maxwell's theory as discussed in terms of thermal conductivity by Eucken. Fig. 6. shows the theoretical variation of the thermal conductivity with volume percent diamond, according to following equation.

$$K_C = K_m \frac{1 + 2V_p \frac{1 - (K_m/K_p)}{1 + (2K_m/K_p)}}{1 - V_p \frac{1 - (K_m/K_p)}{1 + (K_m/K_p)}} \quad (1)$$

where K is thermal conductivity, V_p is volume fraction of diamond, subscript m stands for the α -alumina matrix and p for the diamond particle.

IV. Conclusion

α -alumina/diamond composites have been successfully made by normal hot pressing procedures. These composites possess a fracture toughness, K_{Ic} , which is

considerably higher than the inherent α -alumina matrix, and appreciably lower in thermal expansion coefficients. It also has considerably higher theoretical thermal conductivity, and a higher expected wear resistance. Experimental measurements of the thermal conductivity and thermal shock resistance are planned to verify these theoretical estimations. Furthermore, extensive heat treatment studies and high temperature mechanical properties research are required to determine the effect of the diamond - graphite transformation effects in these composites for high temperature operations. The tribological properties of these composites is also continuing.

Acknowledgment:

We would like to thank Dr. S. A. Howard for his advice and discussions on the Rietveld X-ray diffraction profile analysis.

References

1. A.G. Evans and R.M. McMeeking, "On the Toughening of Ceramics by Strong Reinforcements," *Acta Metall.*, **34** [12] 2435-41 (1986).
2. R.W. Rice, "Mechanisms of Toughness in Ceramic Matrix Composite," *Ceram. Eng. Sci. Pro.*, **2** [7-8] 661-701 (1981).
3. R.P. Wahi and B. Ilschner, "Fracture Behavior of Composites Based on Al_2O_3 -TiC," *J. Mater. Sci.*, **15**, 875-85 (1980).
4. J. Liu and P.D. Ownby, "Enhanced Mechanical Properties of Alumina by Dispersed Titanium Diboride Particulate Inclusions," *J. Am. Ceram. Soc.*, **74** [1] 2213-16 (1991).
5. J. Liu and P.D. Ownby, "Boron Carbide Reinforced Alumina Composites," *J. Am. Ceram. Soc.*, **74** [3] 674-676 (1991).
6. R. M. Chrenko and H. M. Strong, "Physical Properties of Diamond," General Elelctroc CRD Reprt. No.75CRD089, Oct. 1975.
7. K. E. Spear, "Diamond-Ceramic Coating of Future," *J. Am. Ceram. Soc.*, **72** [2] 171-91 (1989).
8. P.D. Ownby and R. W. Stewart, "The Polymorphs of Carbon," ASM Engineered Materials Handbook volume 4, to be published Nov. 1991.
9. P.D. Ownby, US Patent #4968647, issued Nov. 6, 1990.
10. T. Noma and A. Sawaoka, "Effect of Heat Treatment on Fracture Toughness of Alumina-Diamond Composite Sintered at High Pressures," *J. Am. Ceram. Soc.*,

68 [2] C36-C37 (1985).

11. T. Noma and A. Sawaoka, "Toughening in Very High Pressure Sintered Diamond-Alumina Composite of Alumina-Diamond Composite Sintered at High Pressures," *J. Mater. Sci.*, 19, 2319-22 (1984).
12. T. Noma and A. Sawaoka, "Fracture Toughness of High-Pressure Sintered Diamond/Silicon Nitride Composites," *J. Am. Ceram. Soc.*, 68 [2] c36-37 (1985).
13. L.A. Xue and R. Raj, "Effect of Diamond Dispersion on the Superplastic Rheology of Zinc Sulfide," *J. Am. Ceram. Soc.*, 73 [8] 2213-16 (1990).
14. L.M. Barker, "Short Bar Specimens for (K_{Ic}) Measurements"; pp. 73-82 in *Fracture Mechanics Applied to Brittle Materials*, ASTM STP 678. Edited by S. W. Freiman. American Society for Testing and Materials, Philadelphia, PA, 1979.
15. P.D. Ownby, "A Preliminary Study of the Effect of Heat Treatment on the Strength and Microstructure of a Glass-ceramic Materials," MS thesis, University of Missouri-Rolla, (1962).
16. D.L. Bish and S.A. Howard, "Quantitative Phase Analysis Using the Rietveld Method," *J. Appl. Cryst.*, 21 [6] 86-91 (1988).
17. W.J. Lackey, D.P. Stinton, G.A. Cerny, A.C. Schaffhauser, and L.L. Fehrenbacher, "Ceramic Coatings for Advanced Heat Engines-A Review and Projection," *Adv. Ceram. Mat.*, 2 [1] 24-30 (1987).
18. P.D. Ownby and J. Liu, "Nano-Diamond Enhanced Silicon Carbide Matrix Composites," *Ceram. Eng. Sci. Pro.*, (1991).

Table I. Thermal Expansion Coefficients of Alumina/Diamond Composites

diamond volume %	C.T.E. ($\times 10^{-6}/^{\circ}\text{C}$)	
0	7.6	(100 °C-800 °C)
5	6.0	(100 °C-800 °C)
10	5.6	(100 °C-800 °C)
15	5.4	(100 °C-800 °C)
100	1.5-3.8	(100 °C-800 °C) ^a

Figure Captions

- Fig. 1.** Scanning electron micrograph of as-received (a) S-diamond 1/2-1 μm particle powder (b) M-diamond 0-5 μm particle powder.
- Fig. 2.** The X-ray pattern of α -alumina/diamond composites at room temperature.
- Fig. 3.** Density of α -alumina vs volume percent diamond particles.
- Fig. 4.** Fracture toughness of α -alumina vs volume percent diamond particles measured by the CNSR technique.
- Fig. 5.** Diametral tensile strength of α -alumina vs volume percent S-diamond particles.
- Fig. 6.** Theoretical variation of the thermal conductivity with volume percent diamond particles.

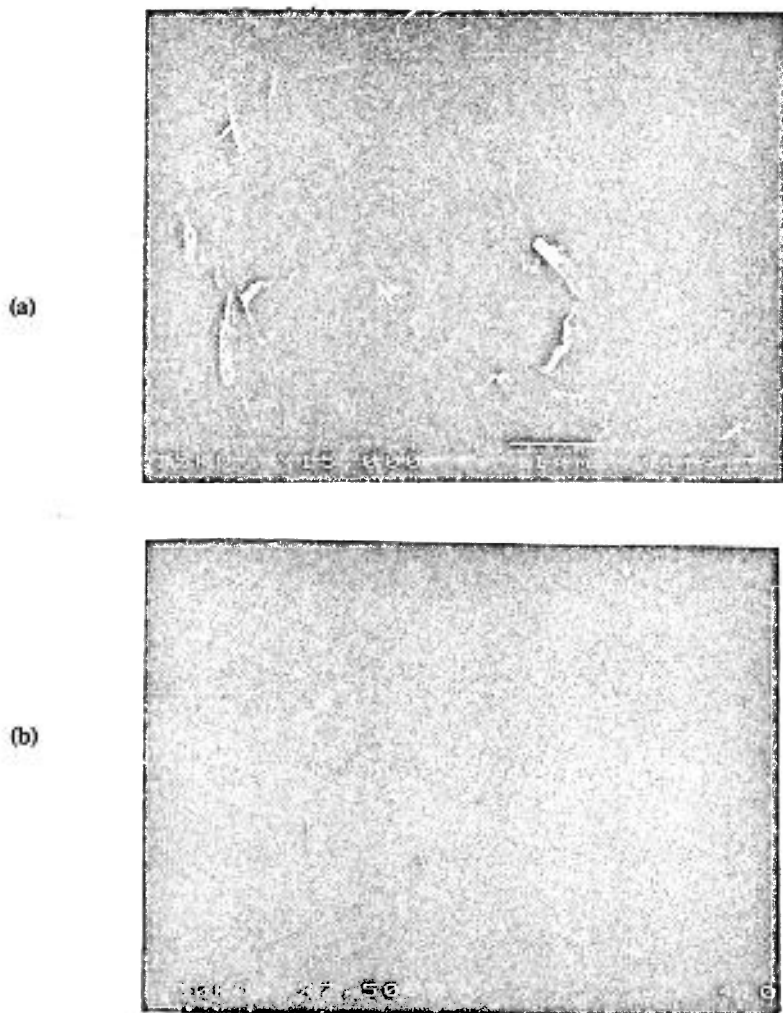


Fig. 1. Scanning electron micrograph of as-received (a) S-diamond 1/2-1 μm particle powder (b) M-diamond 0-5 μm particle powder.

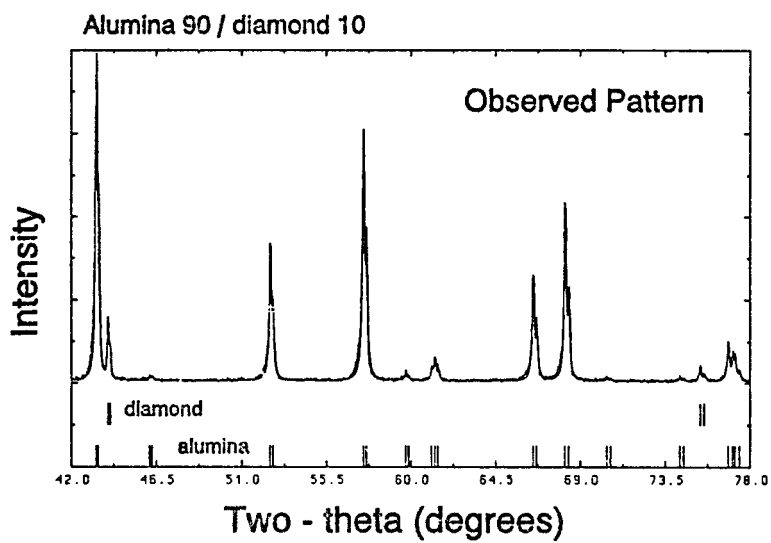


Fig. 2. The X-ray pattern of α -alumina/diamond composites at room temperature.

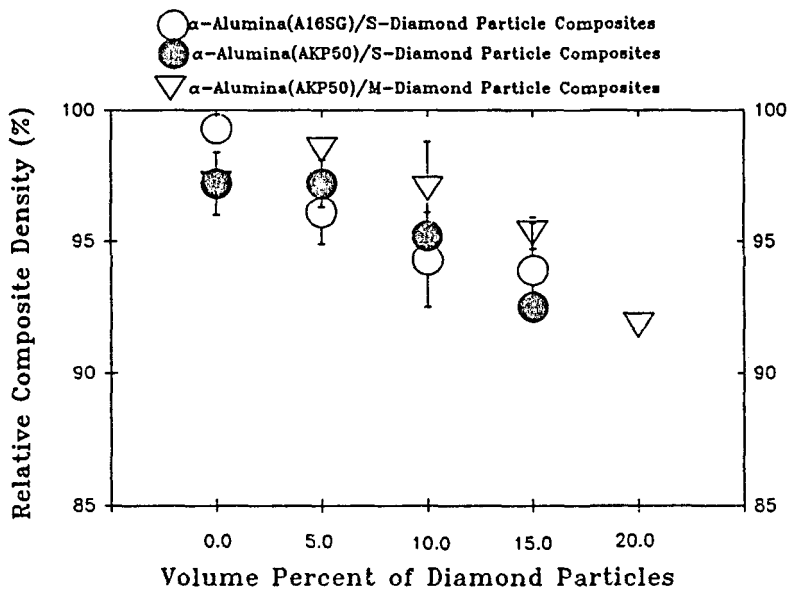


Fig. 3. Density of α -alumina vs volume percent diamond particles.

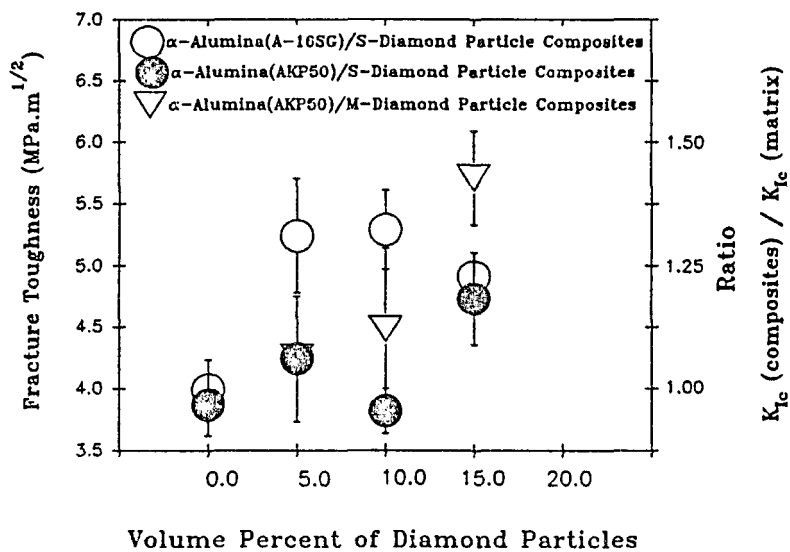


Fig. 4. Fracture toughness of α -alumina vs volume percent diamond particles measured by the CNSR technique.

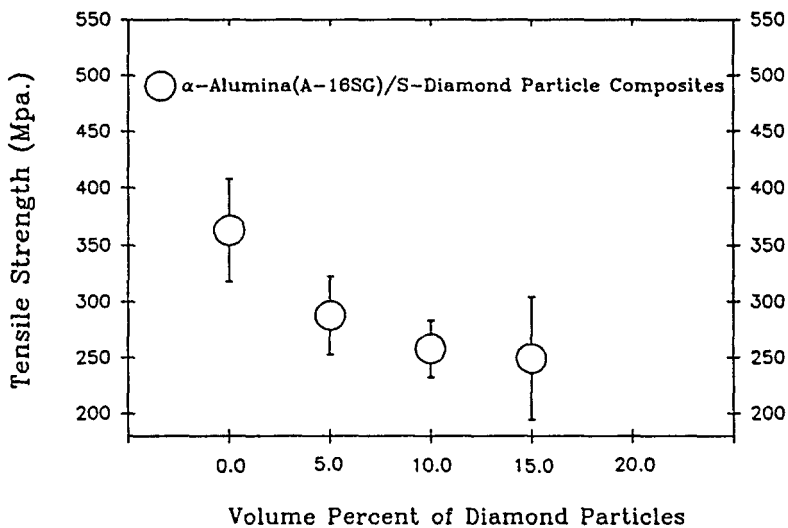


Fig. 5. Diametral tensile strength of α -alumina vs volume percent S-diamond particles.

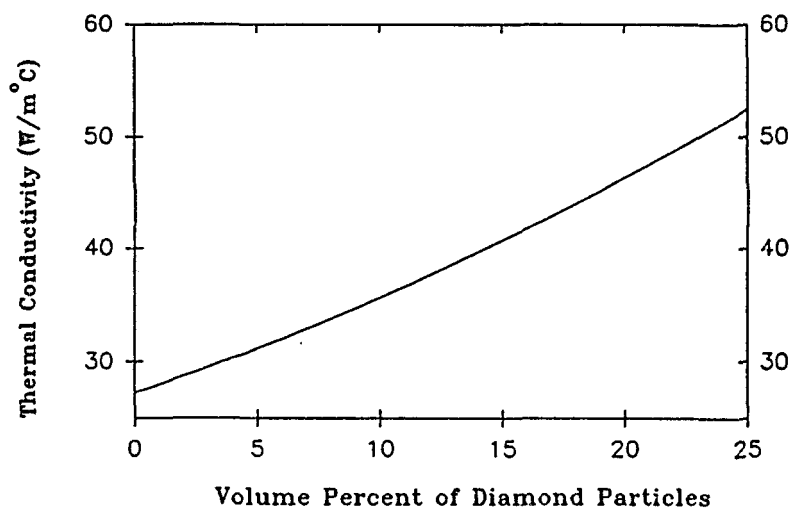


Fig. 6. Theoretical variation of the thermal conductivity with volume percent diamond particles.

PAPER 3**Physical Properties of Alumina-Boron Carbide Whisker/Particle Composites**

Jenq Liu* and P. Darrell Ownby*

Ceramic Engineering Department

University of Missouri-Rolla

Rolla, Missouri 65401

*: members, American Ceramic Society

Physical Properties of Alumina-Boron Carbide Whisker/Particle Composites

Abstract

Alumina-boron carbide composites were prepared by sintering and by hot pressing. The mechanical properties of hot pressed alumina-boron carbide composites are better than the inherent alumina matrix. A maximum fracture toughness, K_{Ic} , of $7.26 \text{ MPam}^{1/2}$ is achieved for alumina-boron carbide whisker composites as is a 47% increase in flexural strength. The fracture toughness is dependent on the volume fraction of boron carbide. The lower thermal expansion coefficient of the composites as a function of boron carbide whisker content is shown.

[Key words: Sintering, Boron carbide particles, Boron carbide whiskers, Alumina, Ceramic matrix composites]

I. Introduction

For toughened ceramic matrix composites, either isolated particles or whiskers are usually chosen as the second phase material.¹ Randomly oriented, well-dispersed particles or whiskers produce composites which have isotropic properties and are relatively easy to fabricate. Individual whiskers usually have higher strength than particles or fibers because of the inherent perfection of these thin single crystals. To be most effective, these discrete, non-reacting additives should have high melting points, higher hardness, higher strength, and higher Young's modulus than the matrix to optimize the fracture toughness enhancing benefit. For high strength ceramic matrices it is difficult to find a material which possesses all of these desirable properties. In the recent literature, silicon carbide^{2,3}, titanium carbide⁴, and titanium diboride⁵ have been selected as the second phase additive to improve the mechanical properties of high density, high strength alumina ceramic matrix composites. However, only silicon carbide and titanium carbide have been available, and therefore utilized, in whisker form. Using these whiskers, non-reacted, two phase composites which show enhanced mechanical properties have been produced in several ceramic matrices which show increased flexural strength, increased fracture toughness, and improved high temperature mechanical properties.⁶

Among high strength, hard ceramic materials, boron carbide has the highest hardness of all except diamond and cubic boron nitride.⁷ It also has the lowest density of all of the super-hard materials. Furthermore, boron carbide possesses the other most desirable

properties including high Young's modulus, lower thermal expansion and chemical compatibility and stability. The recent break-through which has enabled boron carbide to be produced in whisker* form makes it even more attractive. As this commercial process is further developed, better quality whiskers are expected. Because of these unique qualities, alumina-boron carbide composites should be an excellent, light-weight, structural ceramic material candidate with improved mechanical properties compared with other alumina matrix composites .

II. Materials

Boron carbide jet milled particles and the recently developed whiskers have been used in this study. The boron carbide powder particles** as specified ranged in size from 0.2 to 7 μm , which was confirmed by particle size analysis*** and Scanning Electron Microscopy, SEM. The boron carbide whiskers*, as-received, contained a very high more equiaxed particulate content. The whiskers had an aspect ratio of < 15 and the diameter varied greatly from 2 to 15 μm . A16-SG**** alumina powder was used for the matrix.

* Third Millennium Technologies Inc., Knoxville, TN.

** Eagle-Picher Industries Inc., Quapaw, OK.

*** Horiba CCAPA-700, Horiba Ltd., Kyoto, Japan

**** ALCOA-A16SG, Alcoa Industrial Chemicals, Bauxite, AR.

III. Experimental Procedure

Various volume percents of boron carbide whiskers and jet milled powder were thoroughly dispersed in the fine alumina powder in methanol suspension for 2 hours using alumina balls in a plastic jar. These viscous slurries were quickly oven-dried to avoid settling. The alumina/boron carbide granulated powders were sintered at 1500°C and 1600°C for 3 hr and hot pressed at 1520°C for 20 min in boron nitride-coated graphite dies in an argon atmosphere. The sintered and hot pressed specimens were characterized by density, phase content, and microstructure. The mechanical properties of only the high density hot-pressed composites were measured. The densities were measured by the Archimedes method. The fracture toughness, K_{Ic} , was measured by the Chevron Notched Short Rod, (CNSR)^{5,8}, method. The samples were 0.95 cm diameter by 1.43 cm long and fractured parallel to the hot pressing direction. Modulus-Of-Rupture, MOR, three point bend tests were made on 0.5 cm by 0.5 cm by 2.54 cm specimens at a cross-head speed of 0.5 cm/min. The thermal expansion coefficients were measured.*****

The microstructure of the fractured surfaces were analyzed by SEM. Quantitative phase content analysis was accomplished by powder X-ray Rietveld profile fitting⁹.

***** Orton 15BC-1 dilatometer, Orton Inc., Westerville, OH.

IV. Results and Discussion

(1) Density

The sintered and hot pressed composite densities are shown in Fig. 1. The composites could not be sintered to high density with the non-reactive boron carbide second phase inclusions in the Al6SG powder but were limited to less than 80% of the composite density. Work is continuing to achieve high density sintered composites using a higher surface area, more sinterable alumina powder. The hot pressed composite density was >98% of the theoretical composite density.

(2) Mechanical properties

The fracture toughness, K_{Ic} , of hot pressed alumina-boron carbide composites is shown graphically on Fig. 2. Both the whisker and the particle composites show a significant increase in fracture toughness. The K_{Ic} increases more rapidly with the jet milled particle with a maximum at only 5 vol.%. With the whiskers, the fracture toughness continues to increase up to 15 vol.% and remains at a high level with higher whisker content up to 30 vol.%. The advantage of the higher aspect ratio and higher strength whisker is clearly seen.

Resistance to sudden crack propagation, evidenced by these appreciable K_{Ic} values, appears to be associated with crack interactions with the hard boron carbide inclusions and the associated stress redistribution at the crack tip when the particles are

encountered. These interactions include crack bridging¹⁰, grain bridging, crack deflection¹¹, whisker pull-out¹², crack branching and the production of sub-critical microcracks¹³.

The flexural strength of alumina also increases with boron carbide additions as shown in Fig. 3. The MOR for composites with jet milled boron carbide particles exceeds that of the boron carbide whisker/alumina composites. This may be caused by the larger alumina grain size in the whisker containing composites.

These boron carbide whisker reinforced alumina composites rival the well known silicon carbide whisker toughened alumina composites. The fracture strength of the average boron carbide whisker itself, can be calculated from these results as a comparison with the silicon carbide whiskers. This is accomplished by using the dependence of the fracture toughness increase on the whisker strength as derived by Becher et.al¹⁰ as shown in equation (1).

$$\text{equation (1)} \quad \Delta K = \sigma_f \left[\frac{V_f^w r E^c G^m}{6(1-\nu^2) E^w G^i} \right]^{1/2}$$

Where V_f is volume fraction, E is Young's modulus, ν is poisson's ratio, r is radius, G is strain energy release rate, subscript w stands for boron carbide whisker, c for composite, and i for interface. The change in fracture toughness is 3.26 MPam^{1/2} and the ratio $= G^w/G^i = l_p/r$ varies from 1-3 for the composites containing 15 vol.% whiskers. The fracture strength calculated by equation (1) varied from 4-7 GPa. This indicates that the average strength of the boron carbide whiskers is smaller than the silicon carbide whiskers, which have a fracture strength of 10 GPa. The alumina-boron

carbide has a lower thermal expansion coefficient difference compared to the alumina-silicon carbide and, therefore, less residual stress will be developed in these composites.

(3) Microstructure

The polished two phase microstructure of the hot pressed specimens is shown in Fig. 4(a) and (b). The boron carbide was well-dispersed in the alumina matrix. No third phases and no other phases were observed by SEM or reflected light microscopy.

The fractured surface of the CNSR specimens was characterized by SEM. An intergranular fracture surface is observed in the particle composites as shown in Fig. 5(a) providing evidence for the crack-particle interaction mechanisms. The addition of boron carbide whiskers produced a fracture surface which was rougher with a large matrix grain size, and whisker pull-out was observed as shown in Fig. 5(b).

(4) Thermal expansion of alumina-boron carbide composites

The thermal expansion coefficient of alumina is decreased with the addition of the boron carbide whiskers as shown in Table I.

References

1. A.G. Evans and R.M. McMeeking, "On the Toughening of Ceramics by Strong Reinforcements," *Acta Metall.*, **34** [12] 2435-41 (1986).
2. G.C. Wei and P.F. Becher, "Development of SiC-Whisker-Reinforced Ceramics," *Am. Ceram. Soc. Bull.*, **64** [2] 298-304 (1985).
3. S. Lio, M. Watanabe, M. Matsubara, and Y. Matsuo, "Mechanical Properties of Alumina/Silicon Carbide Whisker Composites," *J. Am. Ceram. Soc.*, **72** [10] 1880-1884 (1989).
4. R.P. Wahi, and B. Iischer, "Fracture Behaviour of Composites Based on Al_2O_3 -TiC," *J. Mater. Sci.*, **15**, 875-885 (1980).
5. J. Liu and P.D. Ownby, "Enhanced Mechanical Properties of Alumina by Titanium Diboride Particulate Inclusions," *J. Am. Ceram. Soc.*, **74** [1] 241-43 (1991).
6. J. Homeny, W.L. Vaughn, and M.K. Ferber, "Processing and Mechanical Properties of SiC-Whisker Alumina Composites," *Am. Ceram. Soc. Bull.*, **67** [2] 233-238 (1987).
7. F. Thevenot, "Boron Carbide-A Comprehensive Review," *J. Europ. Ceram. Soc.*, **6** 205-25 (1990).
8. L.M. Barker, "Short Bar Specimens for (K_{Ic}) Measurements,"; pp. 73-82 in *Fracture Mechanics Applied to Brittle Materials*, ASTM STP 678. Edited by S. W. Freiman. American Society for Testing and Materials, Philadelphia, 1979.

9. D.L. Bish and S.A. Howard, "Quantitative Phase Analysis Using the Rietveld Method," *J. Appl. Cryst.*, **21** [6] 86-91 (1988).
10. P.F. Becher, C. Hsueh, P. Angelini and T.N. Tieg, "Toughening Behavior in Whisker-Reinforced Ceramic Matrix Composites," *J. Am. Ceram. Soc.*, **71** [12] 1050-1061 (1989).
11. K.T. Faber and A.G. Evans, "Crack Deflection Processes-I. Theory," *Acta Metall.*, **31** [4] 565-576 (1983).
12. M.D. Thouless and A.G. Evans, "Effect of Pull-out on the Toughness of Reinforced Ceramics," *Acta Metall.*, **36**, 517-521 (1988).
13. Y. Fu and A.G. Evans, "Some Effects of Microcracks on the Mechanical Properties of Brittle Solids-I. Stress, Strain Relations," *Acta Metall.*, **33** [8] 1515-23 (1985).

Table I. Thermal Expansion Coefficients of Alumina-Boron Carbide Whisker Composites

Boron carbide whisker volume %	C.T.E. ($\times 10^{-6}/^{\circ}\text{C}$)
0	7.8 (100°C-800°C)
10	7.6 (100°C-800°C)
20	7.4 (100°C-800°C)
30	7.0 (100°C-800°C)

Figure Captions

Fig. 1. Theoretical composite density (%) versus volume percent boron carbide particles and boron carbide whiskers.

Fig. 2. Fracture toughness of alumina versus volume percent boron carbide particles and boron carbide whiskers.

Fig. 3. Flexural strength of alumina versus volume percent boron carbide particles and boron carbide whiskers.

Fig. 4. Scanning electron micrograph of a polished surface of (a) alumina with 15 vol. % boron carbide powder particles (b) alumina with 15 vol. % boron carbide whiskers.

Fig. 5. Scanning electron micrograph of a fracture surface of (a) intergranular fracture of alumina with 15 vol. % boron carbide powder particles (b) whisker pullout of alumina with 15 vol. % boron carbide whiskers.

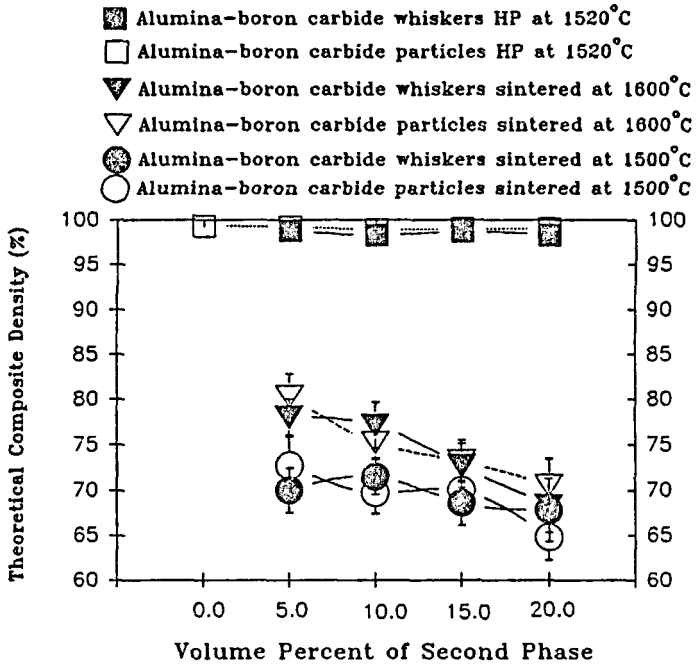


Fig. 1. Theoretical composite density (%) versus volume percent boron carbide particles and boron carbide whiskers.

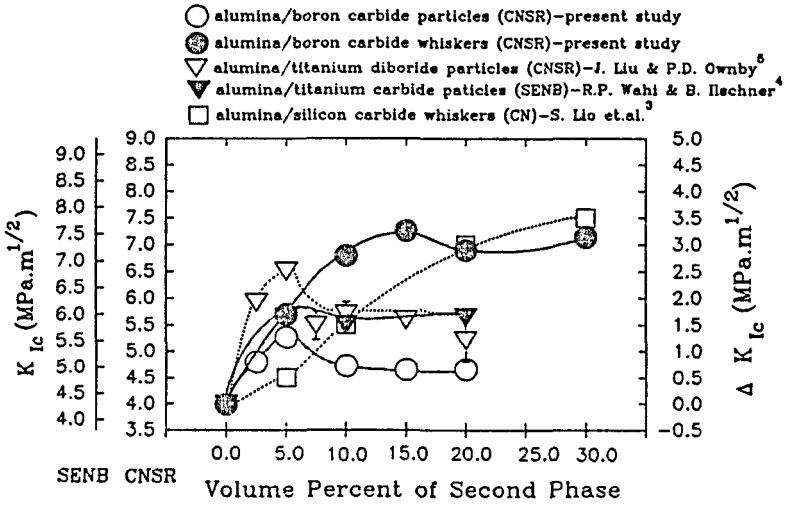


Fig. 2. Fracture toughness of alumina versus volume percent boron carbide particles and boron carbide whiskers.

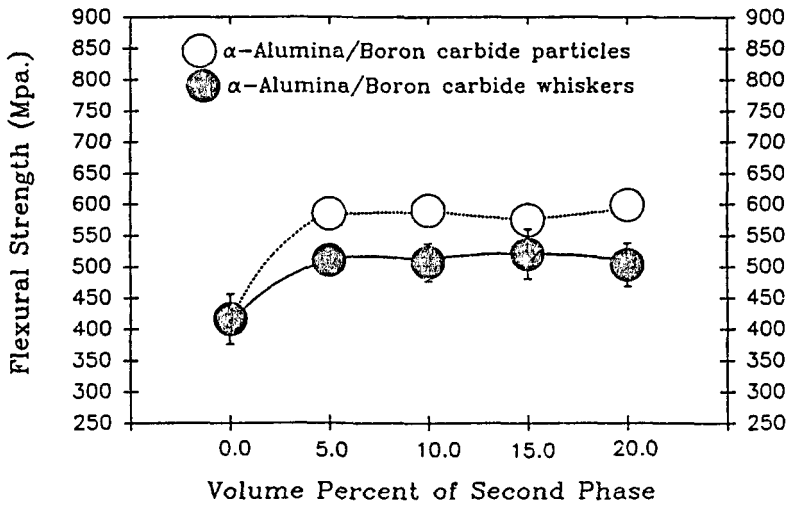


Fig. 3. Flexural strength of alumina versus volume percent boron carbide particles and boron carbide whiskers.

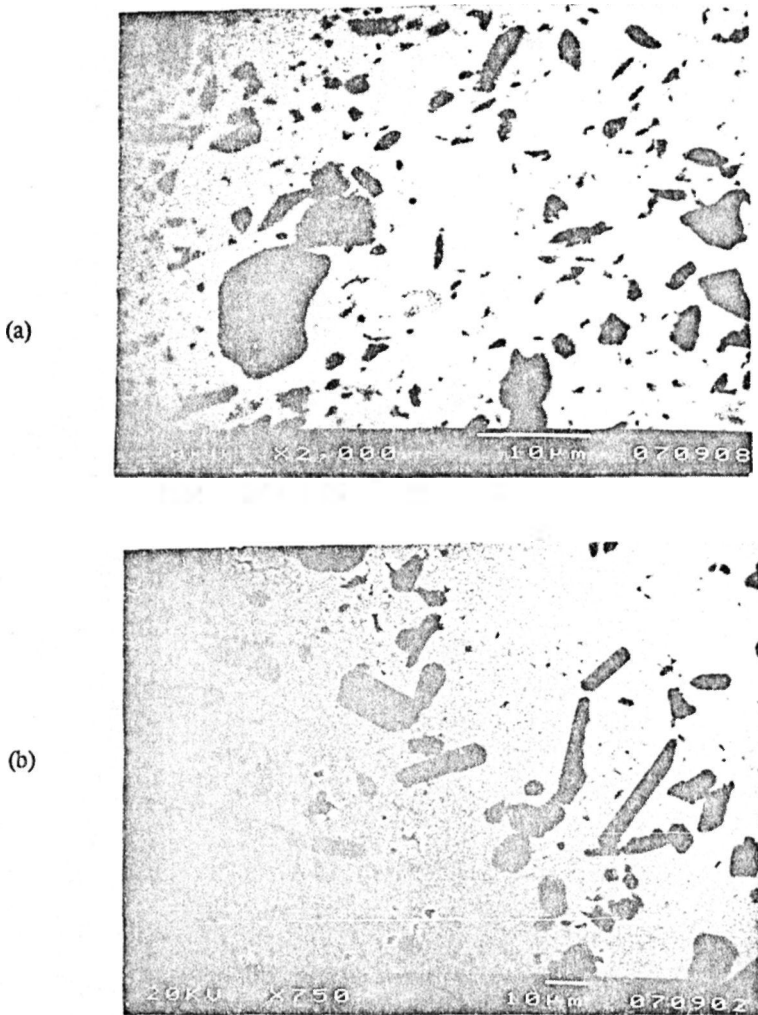


Fig. 4. Scanning electron micrograph of a polished surface of (a) alumina with 15 vol.% boron carbide powder particles (b) alumina with 15 vol.% boron carbide whiskers.

(a)



(b)

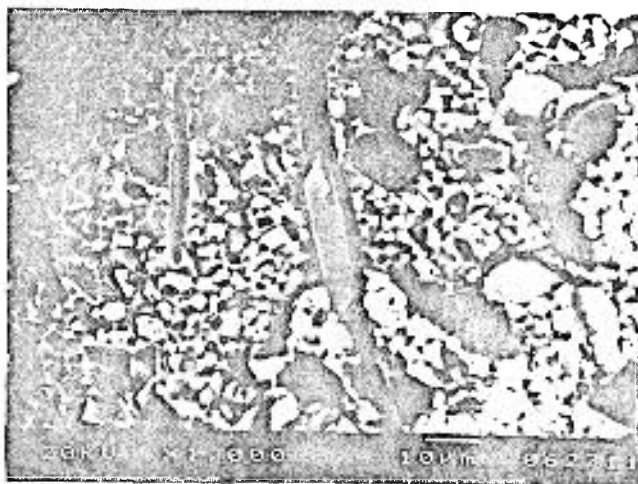


Fig. 5. Scanning electron micrograph of a fracture surface of (a) intergranular fracture of alumina with 15 vol. % boron carbide powder particles (b) whisker pullout of alumina with 15 vol. % boron carbide whiskers.

PAPER 4**Nano-Diamond Enhanced Silicon Carbide Matrix Composites**

P. Darrell Ownby* and Jenq Liu*

Ceramic Engineering Department

University of Missouri-Rolla

Rolla, Missouri 65401

*: members, American Ceramic Society

Nano-Diamond Enhanced Silicon Carbide Matrix Composites

Abstract

The fracture toughness, K_{Ic} , of polycrystalline silicon carbide is shown to be increased more than 100%, up to $7.17 \text{ MPam}^{1/2}$, by the addition of dispersed nano-diamond particles. This K_{Ic} increase is critically dependent on the volume percent and the particle size of the diamond particle. The extremely small size of these isolated diamonds represents, by several orders of magnitude, the smallest particulate toughening agent added as a dispersed powder, as opposed to internal nucleation, ever reported. The toughening mechanisms which are considered are transformation toughening, microcrack toughening, and crack deflection. The significance of the non-cubic diamond polytypes in transformation toughening is discussed. Quantitative analysis of the hexagonal and cubic polytype distribution by Rietveld powder X-ray diffraction profile fitting of the explosively produced diamond of the type used for toughening enhancement is reported. Besides increasing the fracture toughness, the added diamond increases the thermal conductivity by 70% according to theory. It is also expected that the ΔT required to thermal shock the carbide will also be increased. Work is continuing to measure these and other physical properties of these unique composites.

[Key words: Mechanical properties, diamond, silicon carbide, fracture toughness, non-oxide ceramic matrix composites.]

I. Introduction

Silicon carbide possesses many exceptional physical properties which promote its use in several advanced industrial applications. Its high strength, high hardness, and high Young's modulus make silicon carbide valuable as an abrasive and grinding material and also as a reinforcing material to enhance the mechanical properties of ceramic and metal matrix composites. In fact, it is very difficult to select a material which possesses mechanical properties which are better or even rival silicon carbide as a ceramic matrix reinforcing material. Its highly refractory character establishes silicon carbide as a prime candidate for use in high temperature engines. However, its brittle nature limits its development as a high temperature engineering material.

Diamond is unique in possessing very high strength, very high thermal conductivity, an unequalled hardness, and a low thermal expansion coefficient. Secondly, it is chemically compatible with carbide since it is solely carbon itself. Thirdly, its well-known polymorph, graphite, which is stable at ordinary pressures, has a lower density and therefore a higher volume, making transformation toughening possible. These extraordinary physical properties make diamond a most promising candidate as a fracture toughening agent for high strength, high temperature, carbide ceramic matrix composites. In this paper, very small, nano-meter size diamond particles are dispersed in the carbide matrix acting as a fracture toughening agent to enhance the mechanical properties and to increase the thermal conductivity of the silicon carbide matrix at the same time.

The fracture toughening mechanisms which were considered are transformation

toughening, microcrack toughening, and crack deflection. In transformation toughening¹ a displacive transformation tends to occur between the hexagonal diamond polytype(s) and graphite. This increase in volume tends to (a) close a propagating crack which enters the process zone where these inclusions reside, (b) create localized stress centers which may cause microcracking in the matrix around the inclusion or (c) deflect the crack. In microcrack toughening² a residual tensile stress develops microcracks around the dispersed nano-diamond particles to toughen the silicon carbide by extending them sub-critically and thereby absorbing the energy of a propagating crack. In crack deflection³ a crack may be deflected by the diamond inclusion because of its high strength and hardness and/or by the high stress field surrounding it.

II. Experimental Procedure

Sub-micron SiC powder^{*} was mixed with different volume percents and different particle sizes of explosively formed diamond polytype(s)^{**} in aqueous suspensions. The powder suspensions were evaporated during ultrasonic vibration to provide thorough dispersion of the individual diamond particles in the dry powder. This composite powder was pressed at 55 KB. (5.5 GPa.) and 1500°C in a press capable of operation in the diamond stable range.^{***} The pressed specimens were characterized by density, phase

* DENNIC Type 2, Showa Denko K. K., Minato-Ku, Japan

** Dupont Myplex™, E.I. Dupont de Nemours & Co., Gibbstown, New Jersey.

*** Smith Megadiamond, Provo, Utah.

content, microstructure, and mechanical properties. The density was measured by the Archimedes method. Phase content analysis was accomplished by powder X-ray Rietveld profile fitting analysis⁴.

These specimens were polished with 1 μm diamond paste. After polishing, the samples were cleaned in an ultrasonic cleaner to thoroughly remove the polishing media. The fracture toughness stress intensity factor, K_{Ic} , was measured by the Vicker's diamond indentation method⁵ with a 30 Kg load. The stress intensity factor, K_{Ic} , was determined from an average of 5-10 indentations.

III. Results and Discussion

(1) Polytypes of the diamond and silicon carbide

Diamond has been proposed to exhibit several polytypes, 3C**** (cubic diamond), 2H (Lonsdaleite), 4H, 6H, 8H, 10H, 15R, and 21R diamond⁶. These polytypes are identical to those of silicon carbide except the silicon atoms are replaced with carbon⁷. The structural features and notation of the diamond and silicon carbide polytypes are given in Table I. Equilibrium polymorph formation of crystalline materials is dependent on temperature and pressure, but the diamond polytypes are determined also by kinetic factors such as the pressure, load rate and duration. Indeed, non-cubic diamond polytype

**** Ramsdell notation: The unique number of unit stacking layers in sequence in the unit cell, while the letter refer to the cubic (C), hexagonal (H), or rhombohedral (R) symmetry of the structure.

formation is known to be induced by rapid quench rates (CVD) and rapid load rates (explosive compaction). The transformation between the 2H (Lonsdaleite) and graphite is displacive rather than diffusive and involves a large volume increase. This tendency for volume increase of the dispersed diamond particle in the silicon carbide matrix at high use or formation temperature tends to create stress centers around each dispersed carbon particle which may lead to microcracking. Polytypes of the silicon carbide may also promote the nucleation and growth of similar polytypes in the diamond or vice-versa during the densification of the silicon carbide-diamond composites.

(2) Residual stress

A thermal expansion mismatch alone between diamond and silicon carbide [α_{diamond} (CTE=1.3-3.9 $\times 10^{-6}$ °C⁻¹) < α_{SiC} (CTE=4.3-5.6 $\times 10^{-6}$ °C⁻¹)] will develop tangential hoop tensile stress for the matrix and compressive stress in the diamond upon cooling from densification. The hoop tensile stresses produced by this mechanism alone may promote matrix microcracking. Analysis of these residual stresses, the radial matrix stress (σ_{mr}) and the tangential matrix stress ($-2\sigma_{m\theta} = \sigma_{mt}$), is based on the hydrostatic stress (σ_h) developed around the isolated diamond particle, which, for spherical particles, can be calculated by the following equation⁸:

$$q = \sigma_{mr} = \sigma_h = \frac{(\alpha_p - \alpha_m)\Delta T}{\left[\frac{(1+\nu_m)}{2E_m}\right] + \left[\frac{(1-2\nu_p)}{E_p}\right]} \quad (1)$$

where α is thermal expansion coefficient, E is Young's modulus, ν is poisson's ratio, ΔT

is temperature change, subscript m stands for the silicon carbide matrix and p for the diamond particle.

Upon substitution of the appropriate physical parameter values.

$$q=1.73 \text{ GPa.}$$

This value is sufficiently large to cause microcracking.

(3) Crack deflection by diamond particles

When a crack encounters a diamond, the crack may be deflected by the hard diamond particle. This crack deflection is based on the fact that diamond has twice the Young's modulus, strength and fracture toughness of the silicon carbide matrix as shown in Table II².

(4) Thermal conductivity and thermal shock resistance

Diamond has a very high thermal conductivity (5.43 W/cm°C), whereas silicon carbide is much more of a thermal insulator (0.2-0.87 W/cm°C). Therefore, the thermal conductivity of silicon carbide is enhanced by the addition of diamond particles. This makes an already excellent tooling and grinding material even better for many applications since the heat can more readily be conducted away from its interface with the work piece. The thermal shock resistance of the silicon carbide is also enhanced. Experimental work to show the details of these improvements is continuing.

The following treatment displays the expected results according to Maxwell's theory as discussed in terms of thermal conductivity by Eucken. Fig. 1. shows the theoretical

variation of the thermal conductivity with volume percent diamond, according to equation (2).

$$K_c = K_s \frac{1 + 2V_d \frac{1 - (K_j/K_d)}{1 + (2K_j/K_d)}}{1 - V_d \frac{1 - (K_j/K_d)}{1 + (K_j/K_d)}} \quad (2)$$

where K is thermal conductivity, V_d is volume fraction of diamond, subscript s stands for the silicon carbide matrix and d for the diamond particle.

(5) X-ray analysis

The coexistence of diamond-3C and diamond-2H (Lonsdaleite) was found in the as received Mypolex™-diamond. Rietveld powder X-ray diffraction profile fitting of the entire diffraction pattern made quantitative analysis possible. It was performed on 1 μm duPont Mypolex™ and 1 μm GE Man Made™ industrial diamond for comparison. A single major peak of both materials is shown in Fig. 2. Quantitative Rietveld analysis yielded 78 wt% 3C and 22 wt% hexagonal, assuming 2H, for the duPont 1 μm powder and 100 wt% 3C and 0 wt% 2H for the GE 1 μm powder. Rietveld Profile fitting analysis has also revealed that the 3C/2H ratio decreases with decreasing diamond particle size. However, for extremely small particles sizes in the nanometer range, the number of polytypes coexisting in the powder makes quantitative analysis more complex. The efforts to quantify the complicated distribution of all of these polytypes is continuing.

Diamond will transform to graphite¹⁰ at high temperature. In order to prevent

premature graphitization of the diamond, the composite densification is carried out at the high pressure and temperature required to produce diamonds from graphite industrially. Silicon carbide and polycrystalline nano-diamond powders were analyzed by XRD before and after densification. The hot pressed silicon carbide-diamond specimens were found to retain the same silicon carbide and diamond content as in the original powder batch. No graphite within the XRD detection limit could be detected by XRD after composite densification as shown in Fig. 3. Small but significant amounts (<3%) of graphite may be below the detection limit. Although the carbide and the diamond phases could easily be distinguished, the polytypes of both silicon carbide and diamond in the hot pressed composite are difficult to distinguish by XRD analysis and work in this area is also continuing.

(6) Density and Fracture toughness, K_{Ic}

The sintered composite density decreases with addition of the diamond particles, as shown in Fig. 4.

These silicon carbide composite specimens were so small that the fracture toughness could only be measured by the Indentation method. The indentation method is known to produce various results depending on which one of the many possible equations is used. In this paper the equation⁵

$$K_{Ic} = 0.016(E/H)^{1/2} P/c^{3/2}$$

where E is Young's modulus, H is hardness, P is load, c is crack length, was used to calculate the K_{Ic} . This equation has been shown to produce lower values than other

accepted techniques, and was used intentionally to be conservative.¹¹ The fracture toughness results obtained by adding nano-diamond inclusions are expressed graphically in Figs. 5. and 6. The great sensitivity to volume percent diamond added can be seen in Fig. 5. No increase in K_{Ic} is produced at <10% or >30 vol% diamond. A remarkable increase (more than double) is produced between 18 and 25 vol% diamond. The decreased K_{Ic} with diamond >30 vol% may be due to the lower composite density.

Equally striking is the particle size dependence shown in Fig. 6. At 18.5 vol.% diamond, no increase in fracture toughness is observed until the diamond particle size is reduced to 11 nm. Only then does the value double. These extremely small particles are the smallest toughening agents yet reported by several orders of magnitude. Work is continuing to see if the effect continues with even smaller diamond particles.

References

1. P.D. Ownby, "Fracture Toughening of Sintered Diamond and Carbide Ceramics," US Patent #4,968,647, issued Nov. 6, 1990.
2. Y. Fu and A.G. Evans, "Some Effects of Microcracks on the Mechanical Properties of Brittle Solids-I. Stress, Strain Relations," *Acta Metall.*, **33** [8] 1515-23 (1985).
3. K.T. Faber and A.G. Evans, "Crack Deflection Processes-I. Theory," *Acta Metall.*, **31** [4] 565-76 (1983).
4. D.L. Bish and S.A. Howard, "Quantitative Phase Analysis Using the Rietveld Method," *J. Appl. Cryst.*, **21** [6] 86-91 (1988).
5. G.R. Anstis, P. Chantikul B.R. Lawn, and D.B. Marshall, "A Critical Evaluation of Indentation Techniques for Measuring Fracture Toughness: I, Direct Crack Measurement," *J. Am. Ceram. Soc.*, **64** [9] 533-38 (1981).
6. K.E. Spear, A.W. Phelps, and W.B. White, "Diamond Polytypes and their Vibrational Spectra," *J. Mater. Res.*, **5** [11] 2272-85 (1990)
7. J. Selsing, "Internal Stresses in Ceramics," *J. Am. Ceram. Soc.*, **44** [8] 419 (1961).
8. N.W. Jepps and T.F. Page, "Polytypic Transformations in Silicon Carbide," pp259-306 in *Crystal Growth and Characterization of Polytype Structures*, Edited by P. Krishna, Pergamon press, (1983).
9. W.J. Lackey, D.P. Stinton, G.A. Cerny, A.C. Schaffhauser, and L.L. Fehrenbacher, "Ceramic Coatings for Advanced Heat Engines-A Review and Projection," *Adv. Ceram. Mat.*, **2** [1] 24-30 (1987).

10. R. M. Chrenko and H. M. Strong, "Physical Properties of Diamond," General Elelectroc CRD Reprt. No.75CRD089, Oct. 1975.
11. J. Liu and P.D. Ownby, "Enhanced Mechanical Properties of Alumina by Titanium Diboride Particulate Inclusions," *J. Am. Ceram. Soc.*, 73 [1] 241-43 (1991).

Table I. Polytypes of Diamond and Silicon Carbide⁺

Structure of Diamond and Silicon Carbide Ramsdell notation	Layer repeat sequence *	Jagodzinski** notation	Space Group Diamond	Space Group Silicon Carbide	%Hexagonal
3C	<u>ABC/ABC/A..</u>	(k) ₃	FD3M	F43M	0
2H	<u>AA'/AA'/AA'/.</u>	(h) ₂	P6 ₃ /mmc	P6 ₃ /mc	100
4H	<u>AA'C'C/AA'C'C/A..</u>	(hk) ₂	P6 ₃ /mmc	P6 ₃ /mc	50
6H	<u>AA'C'B'BC/AA'B'BC/A..</u>	(hkk) ₂	P6 ₃ /mmc	P6 ₃ /mc	33
8H	<u>AA'C'B'A'ABC/AA'C'B'ABC/A..</u>	(hk ₂ k) ₂	P6 ₃ /mmc	p6 ₃ /mc	25
15R	<u>AA'C'CABB'A'ABCC'B'BC/AA'..</u>	(hkhkk) ₃	R3M	R3M	40
21R	<u>AA'C'B'BCABB'A'C'ABCC'B'A'ABC/AA'C'..</u>	(hk ₂ khkk) ₃	R3M	R3M	29

+: adapted from ref. 6.

*: Each different symbol in the layer repeat sequence is different but all A layer are identical as are all B and etc.

The primed letters are mirror images of the same unprimed letters.

** : This notation designates the type of stacking between adjacent layers. "k" indicates cubic (Kubisch) and h represents hexagonal stacking.

Table II. Physical Properties of Polycrystalline Silicon Carbide, Diamond, and Cubic Boron Nitride

Material	Theor. Density g/cc	Young's Modulus GPa.	Poisson's Ratio	Thermal Expansion $\times 10^{-6}/K$	Vicker or Knoop Hardness GPa.	Transverse Rupture Strength MPa.	Fracture Toughness K_{Ic} MPa.m ^{1/2}	Thermal Conductivity W/cm°C
silicon carbide	3.21	207-440	0.19	4.3-5.6	20-30	500-930	3.5-4.0	0.2-0.87
diamond	3.52	800-925	0.20	1.3-3.9	35-50	850-1550	6.9	5.43
cubic boron nitride*	3.48	900	0.14	4.8-5.8	28-40	860-900	2.8	2.0

* G.E. 100% microcrystalline BN(BZN™)

Figure Captions

- Fig. 1.** Theoretical variation of the thermal conductivity with volume percent diamond.
- Fig. 2.** The coexistence of Diamond-3C and Diamond-2H of as received 1 μm diamond powder.
- Fig. 3.** The results of the XRD analysis of a densified silicon carbide - 31% diamond composite specimen.
- Fig. 4.** Theoretical composite density vs the volume percent of nano-diamond particle addition.
- Fig. 5.** Fracture toughness, K_{Ic} , of silicon carbide with different volume percents of dispersed 11 nm diamond particles measured by the indentation method with a 30 Kg load.
- Fig. 6.** Fracture toughness of silicon carbide with 18.5 volume percent of different particle sizes of diamond measured by the indentation method with a 30 Kg load.

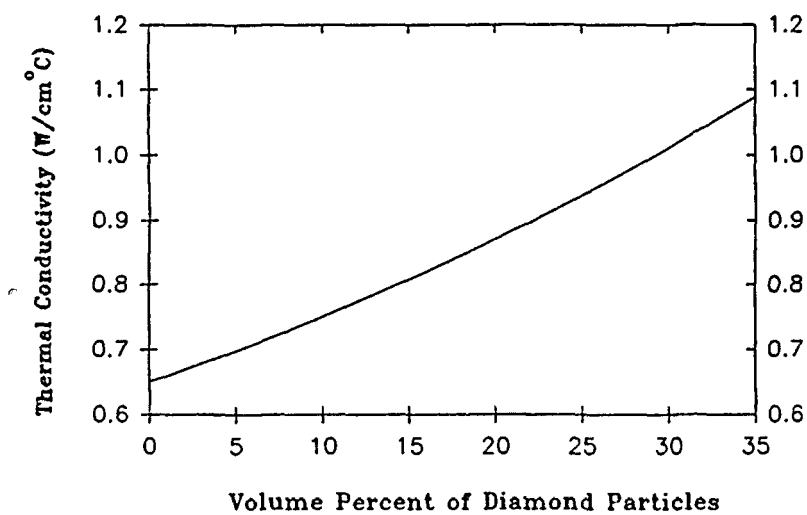


Fig. 1. Theoretical variation of the thermal conductivity with volume percent diamond.

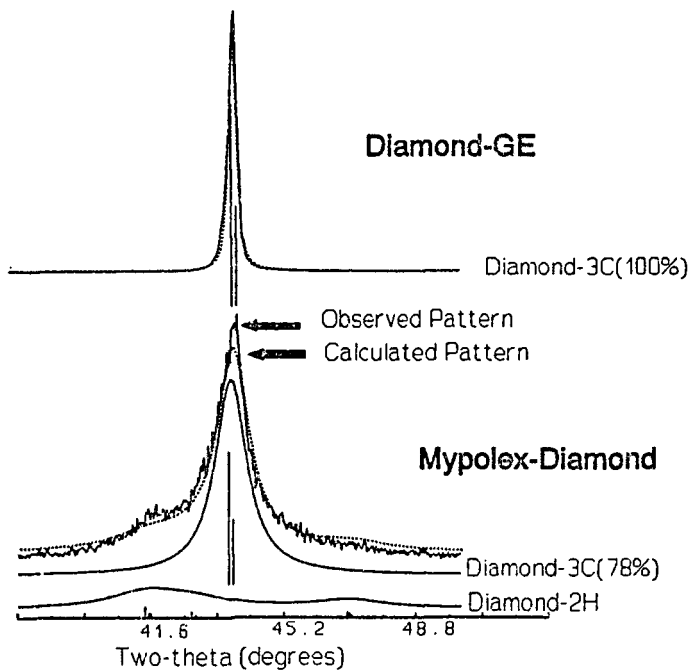


Fig. 2. The coexistence of Diamond-3C and Diamond-2H of as received 1 μm diamond powder.

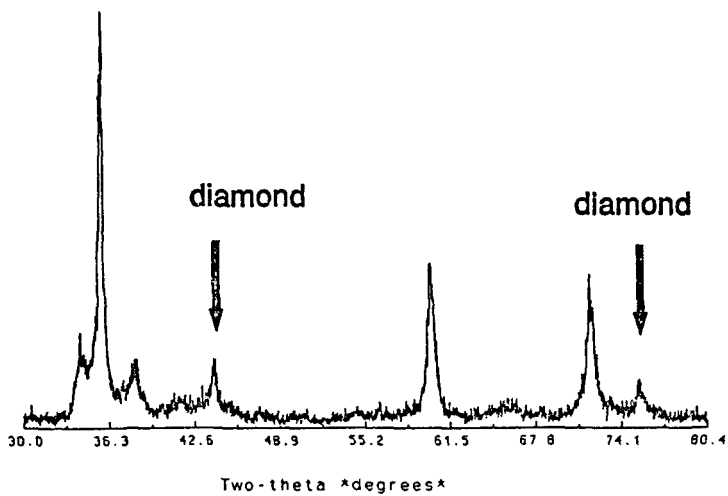


Fig. 3. The results of the XRD analysis of a densified silicon carbide - 31% diamond composite specimen.

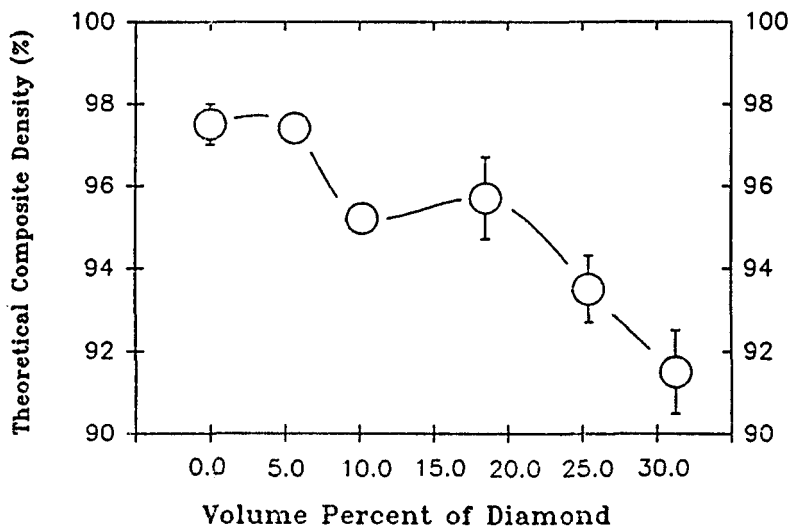


Fig. 4. Theoretical composite density vs the volume percent of nano-diamond particle addition.

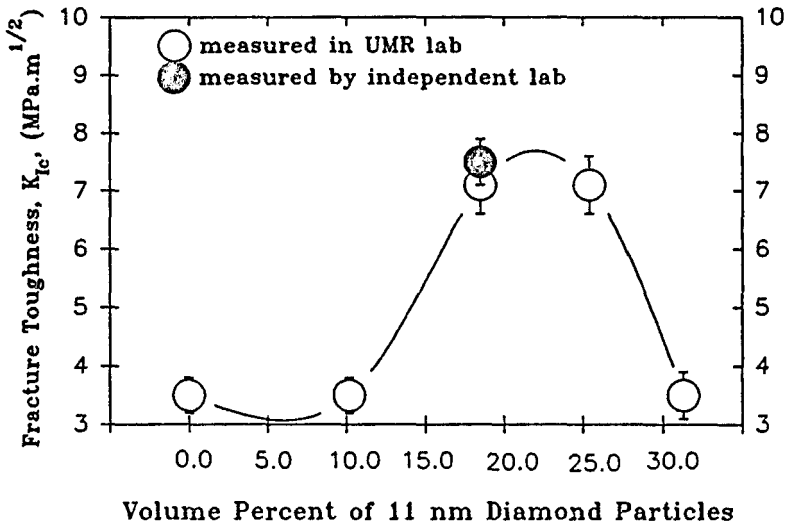


Fig. 5. Fracture toughness, K_{Ic} , of silicon carbide with different volume percents of dispersed 11 nm diamond particles measured by the indentation method with a 30 Kg load.

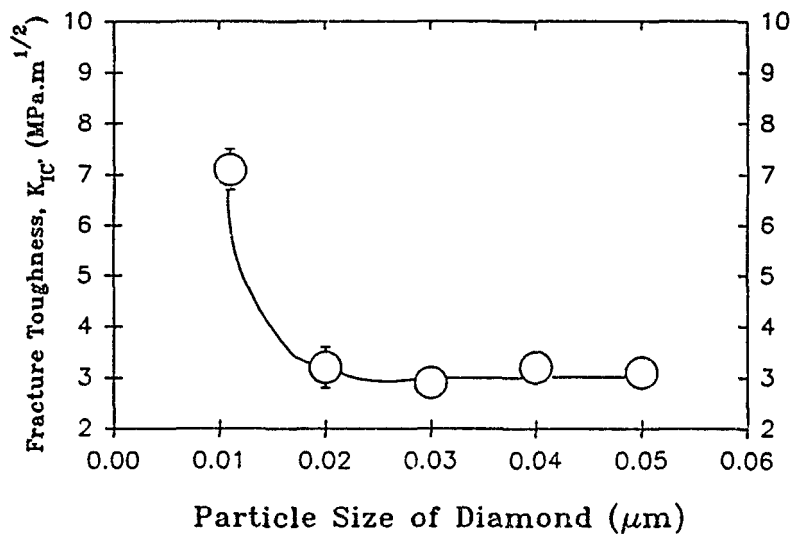


Fig. 6. Fracture toughness of silicon carbide with 18.5 volume percent of different particle sizes of diamond measured by the indentation method with a 30 Kg load.

VITA

Jenq Liu was born on March 2, 1958 in Taipei, Taiwan, where he completed his primary and secondary education. In May 1982 he received his Bachelor of Engineering degree in Chemical Engineering from the Chinese Culture University, in Taipei, Taiwan.

He has been enrolled in the Graduate School of the University of Missouri-Rolla in the Department of Ceramic Engineering since August 1985. Upon completion of his Master of Science degree in Ceramic Engineering in December 1987, he has continued with his doctoral studies at the University. He is member of both Keramos and the American Ceramic Society.

APPENDIX A

Reprint of

Boron Carbide Reinforced Ceramic Matrix Composites

Jenq Liu and P. Darrell Ownby

Boron Carbide Reinforced Alumina Composites

Jenq Liu* and P. Darrell Ownby†

Ceramic Engineering Department, University of Missouri, Rolla, Missouri 65401

The mechanical properties of alumina have been successfully improved by adding isolated boron carbide particles of two different shapes. A K_{Ic} of $7.26 \pm 0.29 \text{ MPa}\cdot\text{m}^{1/2}$ for alumina-boron carbide whiskerlike composites and of $5.27 \pm 0.12 \text{ MPa}\cdot\text{m}^{1/2}$ alumina-boron carbide shardlike particle composites has been achieved. The fracture toughness of these composites is dependent on the volume fraction of the boron carbide particles as well as their size and shape. The flexural strength is also appreciably enhanced to a constant value with from 5 to 20 vol% boron carbide additions. The whiskerlike particles increase the flexural strength by 25% and the shardlike particles produce a 47% improvement. [Key words: mechanical properties, boron carbide, particles, whiskers, alumina.]

I. Introduction

SECOND-PHASE particles or whiskers, which have a large difference in physical properties from the ceramic matrix, have been shown to produce ceramic-matrix composites with improved mechanical properties. For example, in recent years, it has been demonstrated that silicon carbide particles and/or whiskers can act as reinforcing agents to significantly improve the mechanical properties of alumina ceramics.¹⁻³ These composites show enhanced mechanical properties, such as increased flexural strength, increased fracture toughness (K_{Ic}), and improved high-temperature properties. The K_{Ic} enhancement mechanisms have been attributed to crack bridging,¹ crack deflection,² and whisker pullout,³ which occur in the process zone surrounding the crack front.

Boron carbide has the necessary high strength and high Young's modulus required to produce enhanced mechanical properties in alumina ceramics. Furthermore, its exceptional hardness is highest of all materials except diamond and cubic boron nitride and it has the lowest density of all of the superhard materials. The physical properties of alumina, silicon carbide, diamond, cubic boron nitride, and boron carbide are summarized in Table I.⁴ Based on these favorable properties and the crack-particle interaction mechanisms enumerated above, it was postulated that alumina-matrix composites

with well-dispersed, nonequiaxed, boron carbide particles or whiskers would show an increase in fracture toughness and flexural strength. Moreover, these composites would have a lighter weight than other alumina-matrix composites, making them excellent lightweight abrasive material candidates with improved mechanical properties.

II. Experimental Procedure

Boron carbide in the form of fine shardlike morphology powder,⁵ and single-crystal whiskers,⁶ were first characterized by scanning electron microscopy (SEM) to determine their size and shape. The SEM revealed that the as-received "whiskers" contained a very high "shot" or more equiaxed particulate content as shown in Fig. 1(A). The aspect ratio of the "whiskers" was <15 . The diameter varied greatly from 2 to 15 μm . The boron carbide shardlike powder particles ranged in particle size from 0.2 to 7 μm , which was confirmed by particle size analysis.⁷ These particles were irregular in shape, as shown in Fig. 1(B).

Various volume percents of boron carbide "whiskers" and boron carbide shardlike powders were mixed with fine α -alumina powder⁸ in methanol for 2 h using alumina balls in a plastic jar. The resulting slurries were oven-dried. The aspect ratio of the whiskers was not significantly changed, after mixing. The alumina/boron carbide granulated mixed powders were hot-pressed in boron nitride coated graphite dies in argon atmosphere, at 1520°C for 20 min to $>98.0\%$ of the theoretical composite density. The hot-pressed specimens were characterized by density, phase content, microstructure, flexural strength, and fracture toughness. The densities were measured by the Archimedes method. Two different shapes of specimens were hot-pressed for mechanical tests. Short rods were made for chevron notched short rod (CNSR) K_{Ic} determinations.⁹⁻¹² They measured 0.95 cm in diameter by 1.43 cm long and were fractured parallel to the hot-pressing direction. Modulus-of-rupture (MOR) three-point bend tests were made on 0.5 cm \times 0.5 cm \times 2.54 cm, 1 μm diamond polished specimens at a crosshead speed of 0.5 cm/min.

The microstructure of the fractured surfaces and the crack patterns were analyzed by SEM. Precise phase content analysis was accomplished by powder X-ray Rietveld profile fitting.¹³

P. F. Becher—contributing editor

Manuscript No. 197106. Received November 30, 1990; approved January 10, 1991.

*Member, American Ceramic Society.

⁵Esch-Picher Industries, Inc., Osgaw, OK.

⁶Fire Millwright Technologies, Inc., Knoxville, TN.

⁷Nonex CCAPA-700, Horiba, Ltd., Kyoto, Japan.

⁸ALCOA-AlB5G, Alcoa Industrial Chemicals, Bessemer, AR.

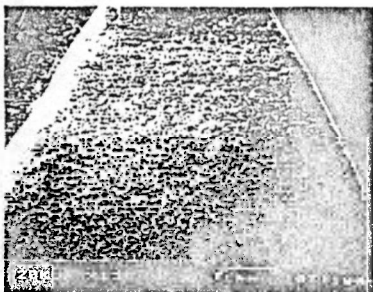
Table I. Physical Properties of Polycrystalline Alumina, Silicon Carbide, Diamond, Cubic Boron Nitride, and Boron Carbide

Material	Theor. density (g/cm ³)	Young's modulus (GPa)	Poisson's ratio	Thermal expansion ($\times 10^{-6}/\text{K}$)	Vickers or Knoop hardness (GPa)	Transverse rupture strength (MPa)	K_{Ic} (MPa·m ^{1/2})
Alumina	3.98	380	0.26	7.2-8.6	18-23	276-1034	2.7-4.2
Silicon carbide	3.21	207-450	0.19	4.3-5.6	20-30	500-930	3.5-4.0
Diamond	3.52	800-925	0.20	1.3-3.9	55-50	850-1550	6.9
Cubic boron nitride*	3.48	900	0.14	4.8-5.3	23-40	860-900	2.8
Boron carbide	2.51	450	0.17	5.0	30-38	300-500	3.8

*G. E. 100% microcrystalline BN(BZN).



(A)



(A)



(B)

Fig. 1. Scanning electron micrograph of as-received (A) boron carbide "whiskers" and (B) boron carbide shardlike particles.

III. Results and Discussion

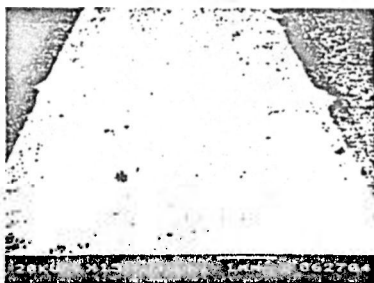
The polished two-phase microstructures of the hot-pressed specimens show that the boron carbide was well dispersed in the alumina matrix. The Rietveld profile analysis detected no third phases and no other phases were observed by SEM or reflected light microscopy. In fact, the Rietveld quantitative analysis agrees with the batch phase composition within 3 wt%, indicative of no detectable boron carbide oxidation.

(1) Microstructure

The fractured surface of the CNSR specimens were characterized by SEM and the results are shown in Fig. 2. The fracture plane of pure alumina was relatively smooth (Fig. 2(A)) with transgranular fracture predominating as shown in Fig. 3(A). The addition of shardlike boron carbide particles produced a rougher surface (Fig. 2(B)) with more intergranular fracture as shown in Fig. 3(B) providing evidence for the crack-particle interaction mechanisms. The addition of boron carbide "whiskers" produced a fracture surface which was even rougher as shown in Fig. 2(C). Whisker pullout was observed as shown in the Fig. 3(C). No increased alumina grain growth was observed on the shardlike boron carbide composites. The grain size was 1 to 2 μm . However, an alumina grain size from 4 to 8 μm was observed on the boron carbide "whisker" containing composites.

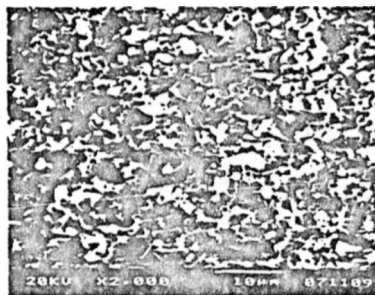


(B)

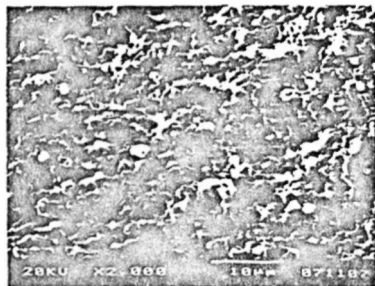


(C)

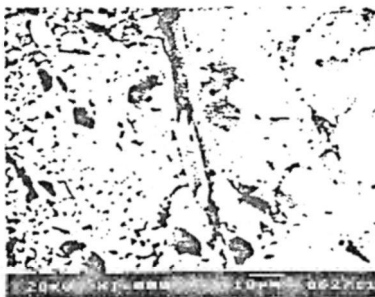
Fig. 2. Scanning electron micrograph of a fracture surface of (A) pure alumina, (B) alumina with 15 vol% boron carbide shardlike particles, and (C) alumina with 15 vol% boron carbide "whiskers."



(A)



(B)



(C)

Fig. 3. Scanning electron micrograph of a fracture surface of (A) transgranular fracture of pure alumina, (B) intergranular fracture of alumina with 15 vol% boron carbide shardlike particles, and (C) whisker pullout of alumina with 15 vol% boron carbide "whiskers."

(2) Mechanical Properties

The K_{Ic} of alumina as a function of volume percent boron carbide additions is presented graphically in Fig. 4. The fracture toughness of alumina reinforced with boron carbide "whiskers" reached $7.26 \pm 0.20 \text{ MPa}\cdot\text{m}^{1/2}$ at 15 vol% boron carbide and was nearly level on further additions of boron carbide "whiskers." This value challenges the alumina-silicon carbide whisker composites, which, with an average diameter of $0.6 \mu\text{m}$ and an aspect ratio of >40 , have a K_{Ic} value that is more than 15% less. The alumina-boron carbide whiskerlike composites have higher K_{Ic} values than any of the previously reported alumina-carbide or -boride particulate composites,^{11,12} in spite of the fact that the "whiskers" used in this study had a very large average diameter, an irregular shape, and were highly contaminated with a wide size range of equiaxed, "shot" particles. With boron carbide shardlike particle reinforced alumina composites, the initial increase in the K_{Ic} curve is similar to the alumina-titanium diboride composites,¹² but different from the alumina-titanium carbide composites.¹⁴ The initial increase in K_{Ic} of alumina-boron carbide composites is less than the alumina-titanium diboride composites and about the same as the alumina-titanium carbide composites up to 5 vol% but surpasses both by nearly 15% at 10 vol%. The fracture toughness of all of these composites is considerably higher than that of the inherent alumina matrix alone.

Resistance to sudden crack propagation is evidenced by the appreciable whisker pullout as seen in Fig. 3(C). Other toughening mechanisms for these composites appear to be associated with the crack interactions with the hard boron carbide inclusions and the associated stress redistribution at the crack tip when the particles are encountered. These interactions can include crack bridging, grain bridging, crack deflection, crack branching, and the production of subcritical microcracks.

The increase of the flexural strength of alumina with boron carbide additions is shown in Fig. 5. The MOR of pure alumina measured here corresponds with the value reported in the literature.¹⁵ The MOR for composites with shardlike boron carbide particles exceeds that of the alumina-boron carbide whiskerlike composites. The lower flexural strength of the boron carbide "whisker" composites may be caused by the larger alumina grain size in these composites.

The K_{Ic} of these boron carbide "whisker" reinforced alumina composites exceeds that of the well-known silicon carbide whisker toughened alumina composites at lower volume percents (≤ 15 vol%). At higher volume percents the shodlike particulate interactions limit the effect of the "whiskers." We anticipate even better results when the quality of the boron carbide whiskers is improved by eliminating

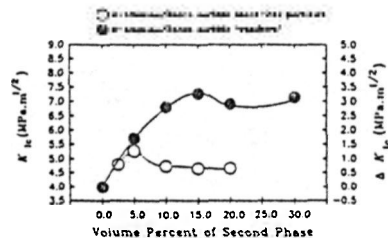


Fig. 4. Fracture toughness of alumina vs volume percent boron carbide shardlike particles and "whiskers" measured by the CNSR technique.

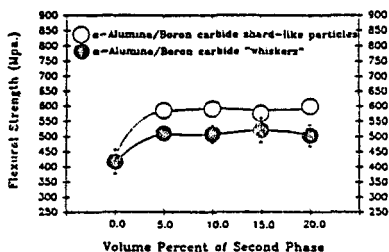


Fig. 5. Flexural strength of alumina vs volume percent boron carbide shardlike particles and boron carbide "whiskers."

the nonwhisker particulate content and increasing the aspect ratio and uniformity of the whiskers.

References

1. P. F. Becher and G. C. Wei, "Toughening Behavior in SiC-Whisker-Reinforced Alumina," *J. Am. Ceram. Soc.*, **67** (12) C-267-C-269 (1984).
2. G. C. Wei and P. F. Becher, "Development of SiC-Whisker-Reinforced Ceramics," *Am. Ceram. Soc. Bull.*, **64** (2) 298-304 (1985).
3. J. Homsey and W. L. Vaughn, "Whisker Reinforced Ceramic Matrix Composites," *MRS Bull.*, **7** (7) 66-71 (1987).
4. J. Homsey, W. L. Vaughn, and M. K. Ferber, "Processing and Mechanical Properties of SiC-Whisker- Al_2O_3 -Matrix Composites," *Am. Ceram. Soc. Bull.*, **66** (2) 333-38 (1987).
5. S. Ito, M. Watanabe, M. Masubara, and Y. Matsuo, "Mechanical Properties of Alumina/Silicon Carbide Whisker Composites," *J. Am. Ceram. Soc.*, **72** (10) 1820-84 (1989).
6. P. F. Becher, C. Haseb, P. Angelini, and T. N. Tiers, "Toughening Behavior in Whisker-Reinforced Ceramic Matrix Composites," *J. Am. Ceram. Soc.*, **71** (12) 1050-61 (1988).
7. K. T. Faber and A. G. Evans, "Crack Deflection Processes—I. Theory," *Acta Metall.*, **31** (4) 565-76 (1983).
8. M. D. Thouless and A. G. Evans, "Effect of Pull-out on the Toughness of Reinforced Ceramics," *Acta Metall.*, **36** (2) 317-21 (1988).
9. J. Lachy, D. P. Sinnott, G. A. Carney, A. C. Schaffhauser, and L. L. Fahrbacker, "Ceramic Coatings for Advanced Heat Engines—A Review and Projection," *Adv. Ceram. Mater.*, **3** (1) 24-30 (1987).
10. M. Barker, "Short Bar Specimens for (K_{Ic}) Measurements," pp. 73-82 in *Fracture Mechanics Applied to Brittle Materials*, ASTM STP 678, Edited by S. W. Freiman, American Society for Testing and Materials, Philadelphia, PA, 1979.
11. J. Liu and P. D. Owensby, "Boron Containing Ceramic Particulate and Whisker Enhancement of the Fracture Toughness of Ceramic Matrix," in *Proceedings of the 20th International Symposium on Boron, Borates and Related Compounds* (Albuquerque, NM, August 27-30, 1990), Edited by D. Emin and T. Aselage, American Institute of Physics, New York, 1991.
12. J. Liu and P. D. Owensby, "Enhanced Mechanical Properties of Alumina by Dispersed Titanium Dioxide Particulate Inclusions," *J. Am. Ceram. Soc.*, **74** (1) 241-43 (1991).
13. D. L. Bish and S. A. Howard, "Quantitative Phase Analysis Using the Rietveld Method," *J. Appl. Crystallogr.*, **21** (6) 86-91 (1988).
14. R. F. Wahl and B. Lischer, "Fracture Behavior of Composites Based on Al_2O_3 -TiC," *J. Mater. Sci.*, **15**, 873-85 (1980).
15. F. E. Buresch, "Fracture Toughness Testing of Alumina," pp. 151-65 in *Fracture Mechanics Applied to Brittle Materials*, ASTM STP 678, Edited by S. W. Freiman, American Society for Testing and Materials, Philadelphia, PA, 1979. □

APPENDIX B

Reprint of

Enhanced Mechanical Properties of Alumina by Dispersed Titanium Diboride Particulate

Inclusions

Jenq Liu and P. Darrell Ownby

Enhanced Mechanical Properties of Alumina by Dispersed Titanium Dioxide Particulate Inclusions

Jenq Liu* and P. Darrell Ownby*

Ceramic Engineering Department, University of Missouri-Rolla, Rolla, Missouri 65401

The mechanical properties of composite ceramics composed of 0 to 20 vol% of titanium dioxide particles dispersed in an α -alumina matrix were investigated. The alumina-titanium dioxide composite powder was hot-pressed at 1470°C for 20 min to achieve over 98.8% of the theoretical composite density. The strength and fracture toughness of the two-phase, hot-pressed composite were both significantly improved compared to the single-phase alumina. Results from different methods of measuring the stress intensity factor, (K_{IC}) are compared and discussed. [Key words: mechanical properties, titanium dioxide, alumina, composites, fracture toughness.]

I. Introduction

The reliability of structural ceramics has been limited by the tendency of ceramics to fail catastrophically by the growth of single cracks originating from small defects, resulting in variable strength and low fracture toughness. Recently, however, mechanical properties of ceramic materials have been improved by the addition of a second phase of small dispersed particles. These second-phase particles can lead to various crack-particle interactions.¹⁻³ Silicon carbide,⁴ diamond,⁵ titanium carbide,⁶ and boron carbide⁷ particles have previously been added to the alumina matrix as hard particles to interact with the crack propagation.

Based on crack-particle interaction mechanisms, it was reasoned that an alumina matrix composite with dispersed, nonequipped, titanium dioxide particles would show an increase in fracture toughness and flexural strength. Titanium dioxide has been shown to successfully enhance the fracture toughness of a silicon carbide matrix.^{1,9}

In the present study, various concentrations (in vol%) of titanium dioxide particles were added to alumina. Fracture toughness was measured on the densified composite using three different methods to compare both the absolute values and relative scatter in the data.

II. Experimental Procedure

Fine alumina powder* and various concentrations of 1- to 15- μ m jet-milled titanium dioxide powder with a mean-particle size of 3 μ m were mixed in a ball mill in ethanol for 2 h using alumina balls in a plastic jar. The resulting slurries were oven dried.

The alumina-titanium dioxide granulated powders were hot-pressed in boron nitride-coated graphite dies at 1470°C

for 20 min, to achieve high-density composites with >98.8% of the theoretical composite density. Two different shapes of hot-pressed specimens were made for mechanical property tests. The applied pressure was 32 MPa for single edge notch beam (SENB) and modulus-of-rupture (MOR) three-point bend tests bars. Short rods were pressed at 64 MPa for both the chevron notched short rod (CNSR) fracture toughness (K_{IC}) determinations and the Vicker diamond indentation (DCMI) fracture toughness tests. Each of the mechanical property measurements reported in this paper represent the average from five to seven specimens and the error bars represent one standard deviation from the mean. The specimens were characterized by density, phase content, microstructure, and mechanical properties. The density was measured by the Archimedes method. All flexure bars and rods were polished and cleaned for mechanical property tests. The short-bar specimens were diamond cut and ground into 0.5 cm \times 0.5 cm \times 2.54 cm flexure bars. The three-point MOR tests were conducted with a span of 1.9 cm at a crosshead speed of 0.05 cm/min to measure the flexural strength. Some specimens were aligned with the bending axis perpendicular and some parallel to the hot-pressed direction axis. A 0.15-cm notch depth was cut in the SENB bars.¹⁰

The CNSR test was accomplished using a fractometer* system. The close-tolerance, chevron-notched specimens were mounted on a flatjack, as shown in Fig. 1, which provides the force to fracture the specimen in a controlled fashion. The K_{IC} and the displacement were recorded with a X-Y recorder.¹¹

Vickers diamond indentations were made on diamond-polished-specimen surfaces with a load of 30 kg for a third measurement of the fracture toughness.¹²

The microstructure of the fracture surfaces and the crack patterns were analyzed by scanning electron microscopy (SEM). Precise phase content analysis was accomplished by powder X-ray Rietveld profile fitting.¹³

*Fractometer I, Terra Test Systems, Inc., Salt Lake City, UT.

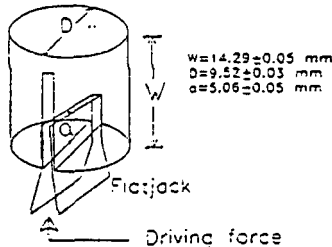


Fig. 1. Specimen for determining K_{IC} by the chevron-notched short-rod method.

R.W. Rice — contributing editor

Manuscript No. 197435, Received July 18, 1990; approved October 25, 1990.

Presented at the 72nd Annual Meeting of the American Ceramic Society, Dallas, TX, April 23, 1990 (Symposium on Ceramic Matrix Composites, Paper No. 88-S1V-90).

*Member, American Ceramic Society.

*ALCOA-Al65G, Alcoa Industrial Chemicals, Baytown, AR.

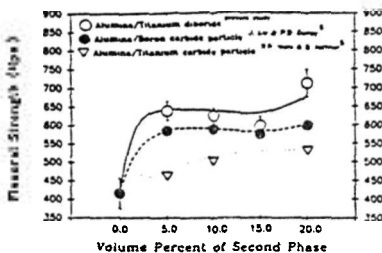


Fig. 2. Flexural strength (MOR) of the alumina matrix composite versus concentration of second-phase particles.

III. Results and Discussions

No third phase could be detected in the composite specimens by Rietveld X-Ray analysis. The titanium diboride particles were observed to be well dispersed in the alumina matrix and no other phases were observed by reflected light microscopy or by SEM. The thermodynamic and chemical stability of titanium diboride in the alumina matrix allows these hard particles to provide improved mechanical properties without the loss of the essential properties inherent in the alumina matrix.

(D) Mechanical Properties

The abruptly increasing flexural strength of alumina with various concentrations of titanium diboride particles is shown in Fig. 2. The MOR of pure alumina measured here corresponds with the value reported in the literature.¹¹ The highest MOR observed was 712 MPa in a composite containing 20 vol% titanium diboride. Comparative results with other second-phase particle inclusions which have been reported on reinforcement alumina matrix composites are also shown in the Fig. 2.

Since the measured value of fracture toughness depends on the measurement method, the results from all three methods are expressed on the left ordinate scales of Fig. 3. The normalized fracture toughness change is shown on the right-hand scale. The indentation method (DCM) is known to produce various results depending on which one of the many possible equations is used. In this paper the equation¹²

$$K_{Ic} = 0.016(E/H)^{1/2} P/c^{3/2} \quad (1)$$

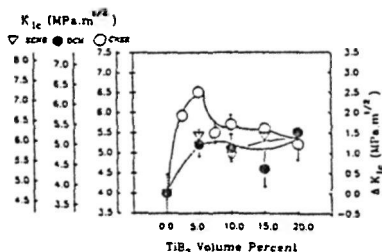


Fig. 3. Fracture toughness (K_{Ic}) of the alumina matrix composite versus concentration of titanium diboride particles added.

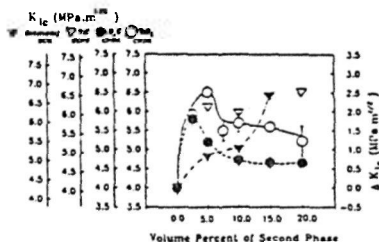
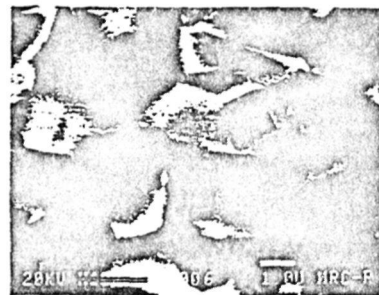


Fig. 4. Fracture toughness (K_{Ic}) of alumina with additions of various toughening agents.



(a)



(b)

Fig. 5. (a) Fracture surface of a CNSR specimen of alumina without second-phase particles additions (bar = 1.0 μm), and (b) fracture surface of a CNSR specimen of alumina with 10 vol% titanium diboride (bar = 1.0 μm).

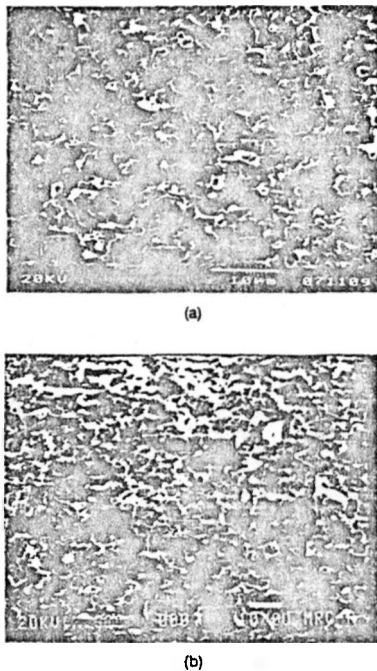


Fig. 4. SEM of the CNSR fracture surface of (a) unmodified alumina matrix (bar = 10 μm), and (b) alumina with 15 vol% titanium diboride (bar = 10.0 μm).

where E is Young's modulus, H is hardness, P is load, and c is crack length, was used to calculate the K_{Ic} . It yields more conservative values than other indentation equations which have been used, but it shows the same trend of fracture toughness increase as in the SENB and CNSR methods. The values measured by the SENB three-point-bending tests and CNSR methods show similarly increasing K_{Ic} , but the CNSR data exhibits much less scatter and a much higher K_{Ic} value at 5 vol% titanium diboride.

The operative toughening mechanisms are considered to be related to crack interactions with the hard titanium diboride

particles. These interactions may include crack deflection and crack bridging, with associated stress redistribution at the crack tip when the particles are encountered. Other mechanisms, such as subcritical microcracks and crack branching around the titanium diboride particles, are also possible contributors to the significant increase in fracture toughness. These irregular jet-milled titanium diboride particles have an increased aspect ratio which may increase the deflection angle.

The mechanical properties of the alumina have been improved by adding the titanium diboride particles. Both the fracture toughness (K_{Ic}) and the flexural strength are significantly improved with only 5 vol% titanium diboride in the alumina matrix. The resulting increase in the fracture toughness of alumina caused by additions of titanium diboride particles in comparison to other hard particle additions is shown in Fig. 4.

(2) Microstructure

SEM of the fracture surfaces of some CNSR specimens is shown in Figs. 5 and 6. Figure 5 shows that the grain size does not change appreciably with titanium diboride additions. Both Figs. 5 and 6 show that titanium diboride promotes more intergranular fracture which is consistent with crack-particle interaction fracture toughening.

References

1. A. G. Evans and R. M. Cannon, "Toughening of Brittle Solids by Martensite Transformations," *Acta Metall.*, 34 [5] 761-760 (1986).
2. A. G. Evans and R. M. McMeeking, "On the Toughening of Ceramics by Strong Reinforcements," *Acta Metall.*, 34 [12] 2435-41 (1986).
3. A. Nakahira, K. Niihara, and T. Hirai, "Microstructure and Mechanical Properties of Al_2O_3 -SiC Composites," *Yogyo Kwakashi*, 94 [8] 767-72 (1986).
4. T. Noma and A. Sawada, "Effect of Heat Treatment on Fracture Toughness of Alumina-Diamond Composites Sintered at High Pressures," *J. Am. Ceram. Soc.*, 68 [2] C-36-C-37 (1985).
5. R. P. Wahl and B. Ilchner, "Fracture Behavior of Composites Based on Al_2O_3 -TiC," *J. Mater. Sci.*, 15, 875-83 (1980).
6. J. Liu and P. D. Oswby, "Boron Containing Ceramic Particulate and Whisker Enhancement of the Fracture Toughness of Ceramic Matrix," in Proceedings of the 10th International Symposium on Boron, Borides, and Related Compounds (Albuquerque, NM, August 27-30, 1990), Edited by D. Emin and T. Aselage, American Institute of Physics, New York, 1991.
7. M. A. Janey, "Mechanical Properties and Oxidation Behavior of a Hot-Pressed SiC-15-wt%-TiB₂ Composite," *Am. Ceram. Soc. Bull.*, 66 [2] 322-24 (1987).
8. H. McMurtry, W. D. G. Boecker, S. G. Seshadri, and J. S. Zhang, "Microstructure and Material Properties of SiC-TiB₂ Particulate Composite," *Am. Ceram. Soc. Bull.*, 66 [2] 325-29 (1987).
9. E. Stawley, "Wide Range Stress Intensity Factor Expressions for ASTM E399 Standard Fracture Toughness Specimens," *Int. J. Fract.*, 12, 457-76 (1976).
10. L. M. Barker, "Short Bar Specimens for K_{Ic} Measurements," pp. 73-82 in *Fracture Mechanics Applied to Brittle Materials*, ASTM STP 678, Ed. by S. W. Freiman, American Society for Testing and Materials, Philadelphia, PA, 1979.
11. G. R. Anstis, P. Chantikul, B. R. Lawn, and D. B. Marshall, "A Critical Evaluation of Indentation Techniques for Measuring Fracture Toughness: I, Direct Crack Measurement," *J. Am. Ceram. Soc.*, 64 [9] 532-38 (1981).
12. D. L. Bish and S. A. Howard, "Quantitative Phase Analysis Using the Rietveld Method," *J. Appl. Crystallogr.*, 21 (Part 2) [4] 79-212 (1988).
13. F. E. Buresch, "Fracture Toughness Testing of Alumina," pp. 151-65 in *Fracture Mechanics Applied to Brittle Materials*, ASTM STP 678, Edited by S. W. Freiman, American Society for Testing and Materials, Philadelphia, PA, 1979. □